

**DESIGN OF STATE PLANE TRAJECTORY CONTROL
FOR A SOFT SWITCHING AC-LINK DC-DC CONVERTER**

by

Jacob Friedrich

B.S. in Electrical Engineering, Gannon University, 2016

Submitted to the Graduate Faculty of
Swanson School of Engineering in partial fulfillment
of the requirements for the degree of
Master of Science

University of Pittsburgh

2018

UNIVERSITY OF PITTSBURGH
SWANSON SCHOOL OF ENGINEERING

This thesis was presented

by

Jacob Friedrich

It was defended on

May 29, 2018

and approved by

Dr. Brandon Grainger, PhD., Assistant Professor, Department of Electrical and Computer
Engineering

Dr. Alexis Kwasinski, PhD., Associate Professor, Department of Electrical and Computer
Engineering

Dr. Gregory Reed, PhD., Professor, Department of Electrical and Computer Engineering

Thesis Advisor: Dr. Brandon Grainger, PhD., Assistant Professor, Department of Electrical
and Computer Engineering

Copyright © by Jacob Friedrich

2018

**DESIGN OF STATE PLANE TRAJECTORY CONTROL FOR A SOFT SWITCHING
AC-LINK DC-DC CONVERTER**

Jacob Friedrich, M.S.

University of Pittsburgh, 2018

The objective of this work is to present the controller operation and mathematical analysis of the AC-link dc-dc converter, a parallel resonant converter, for which state plane trajectory control (SPTC) is proposed. The contribution is an autonomous control technique achieving the benefits of bidirectional power flow, soft switching, and converter switching at its natural resonant frequency as opposed to conventional forced control operations. The switching sequence is implemented using an autonomous state machine triggered by the voltage and current state variables of the resonant LC tank, transitioning between modes of operation strategically to achieve said benefits. By using state plane analysis techniques, the dynamics of the resonant tank can be seen visually, and the trajectories can serve as information to control the converter. All results were simulated in MATLAB/Simulink utilizing the PLECS blockset. In addition, an electrical characteristic study was performed in ANSYS SImplorer on the electrical components to measure the efficiency and thermal response of the semiconductor devices.

TABLE OF CONTENTS

PREFACE.....	IX
1.0 INTRODUCTION.....	1
1.1 BACKGROUND OF AC-LINK CONVERTER.....	1
1.2 RESONANT CONTROLLER TECHNIQUES.....	8
2.0 STATE PLANE TRAJECTORY	13
2.1 EQUIVALENT CIRCUITS FOR DC-DC AC-LINK CONVERTER.....	16
2.1.1 Mode 1 – Charging with Positive Polarity.....	17
2.1.2 Mode 2, 4, 6, and 8 – Resonance.....	19
2.1.3 Mode 7 – Discharging with Negative Polarity.....	21
3.0 OPERATION OF DC-DC AC-LINK CONVERTER	23
3.1 BEHAVIOR OF AC-LINK CONVERTER IN DIFFERENT MODES WITH TRAJECTORIES.....	27
4.0 STATE PLANE TRAJECTORY SWITCHING SEQUENCE	31
4.1 SWITCH SEQUENCE LOGIC.....	34
5.0 SIMULATION RESULTS AND DISCUSSION	38
5.1 SIMULATIONS FOR TRANSIENT EVENTS IN BOOST MODE	42
6.0 THERMAL RESPONSE IN DC-DC AC-LINK CONVERTER USING SPTC..	48
6.1 THERMAL MODELING OF CONVERTER IN BUCK MODE	49
7.0 CONCLUSION.....	54
BIBLIOGRAPHY	55

LIST OF TABLES

Table 1: Normalization Conversion Chart.....	15
Table 2: Converter parameters for bidirectional simulations	38
Table 3: Simulation conditions for boost mode in transient events.....	43
Table 4: Converter parameters for thermal analysis for AC-link converter	49

LIST OF FIGURES

Figure 1:1 Bidirectional dc-dc AC-link topology [1]	4
Figure 1:2: Evaluation of three common capacitors [13]	5
Figure 1:3: Hard switching vs soft switching in semiconductor.....	6
Figure 1:4: AC-link parallel resonant tank's characteristics at specific L and C values	7
Figure 1:5: Example of SPTC on normalized current vs voltage plot with 1:1 voltage transfer..	12
Figure 2:1: Equivalent circuit for mode 1	17
Figure 2:2: State plane trajectory for mode 1	18
Figure 2:3: Equivalent circuit for mode 2.....	19
Figure 2:4: State plane trajectory for mode 2	20
Figure 2:5: Equivalent circuit for mode 7.....	21
Figure 2:6: State plane trajectory for mode 7	22
Figure 3:1: Theoretical output at AC-link converter neglecting resonant modes [2]	24
Figure 3:2: Theoretical output at AC-link with resonant modes in boost mode [2].....	25
Figure 3:3: Operation of mode 1 with corresponding trajectory	28
Figure 3:4: Operation of modes 2, 4, 6, and 8 with corresponding trajectory	28
Figure 3:5: Operation of mode 7 with corresponding trajectory	29
Figure 4:1: Theoretical combined state plane trajectory during boost mode of operation	32

Figure 4:2: Theoretical combined state plane trajectory during buck mode of operation	33
Figure 4:3: State machine for SPTC for AC-Link converter	34
Figure 4:4: System logic for buck and boost modes of operation for state machine controller ...	35
Figure 5:1: Switching Schemes for IGBTs with resonant tank voltage and current waveforms for boost operation.....	39
Figure 5:2: Source 1 and source 2 RMS voltage and current waveforms with different directions of power flow	41
Figure 5:3: State plane trajectories for buck and boost modes of operation.....	42
Figure 5:4: Switching Schemes for IGBTs displaying ZVS in <i>condition 3</i> during boost mode ..	45
Figure 5:5: State Plane Trajectory for AC-Link resonant tank's recovery after transient events during <i>boost</i> mode (green – cond. 1, red – cond. 2, black – cond. 3).....	46
Figure 5:6: State Plane Trajectory for AC-Link resonant tank's recovery after transient events during <i>buck</i> mode (green – cond. 1, red – cond. 2, black – cond. 3).....	47
Figure 6:1: Switch 1 and Switch 3's voltage, current, and gate input waveforms in buck mode.	51
Figure 6:2: Switch 2 and Switch 4's voltage, current, and gate input waveforms in buck mode .	51
Figure 6:3: Switch 5 and Switch 7's voltage, current, and gate input waveforms in buck mode .	52
Figure 6:4: Switch 6 and Switch 8's voltage, current, and gate input waveforms in buck mode .	52
Figure 6:5: Temperature plots for the IGBTs during buck mode	53

PREFACE

First, I would like to express my deepest gratitude to my advisor, Dr. Brandon Grainger. He is the one who truly influenced me to conduct my research in the power electronics field. His persistence and continuous counseling helped me become the researcher I am today. I would also like to thank Dr. Gregory Reed for his gracious support from the first day I arrived at the University of Pittsburgh. I also thank Dr. Alexis Kwasinski for serving on my thesis committee and helping me develop additional insights in power electronics.

I want to thank everyone within the Electric Power Systems Laboratory: Patrick Lewis, J.J. Petti, Ansel Barchowsky, Thomas Cook, Hashim Al Hassan, Alvaro Cardoza, Zachary Smith, Chris Scioscia, Santino Graziani, Andrew Bulman, Matthieu Bertin, Samantha Morello, Dr. Katrina Kelly-Pitou, and Carrie Snell for all their support and camaraderie. In addition, I would like to extend a special thanks to Ryan Brody for assisting me as an undergraduate researcher. The conversations and laughs I endured throughout my time within the windowless lab are unforgettable.

I would also like to show appreciation for the generosity of the Hillman Family Foundation for their financial support of my tuition, which allowed me to explore many research avenues and grow as an engineer with no financial burdens.

Finally, I want to thank my family for their love and continued support throughout all of my education and occasional complaining.

1.0 INTRODUCTION

This chapter presents the main motivation and background material for this work. The dc-dc AC-link converter is investigated, as well as, similar bidirectional circuit topologies. The benefits and challenges of resonant converters and soft switching characteristics are described. A literature review of the details of the research conducted is provided.

1.1 BACKGROUND OF AC-LINK CONVERTER

In this thesis, the topology AC-link converter is introduced with a specialized controller while using state-plane analysis. This converter was first introduced through [1] and [2] and it contains many benefits that are valuable for renewable energy applications, electric vehicles, and microgrids. These benefits include, but are not limited to, the ability to operate at high switching frequencies, soft switching, and bidirectional power flow. With the increasing presence of smart electrification in every day appliances, the need for better circuit topologies and control methods are proliferating.

The evolution of the bidirectional converters generally comes from isolated unidirectional power converts, such as the flyback, buck-boost, half-bridge, and full-bridge converters [3]. This is because the basis of these structures can withstand high and low voltages, which make the

topologies considerable candidates for bidirectional capabilities. Many dc-dc converters are available on the market that can provide exceptional results.

One popular bidirectional converter is the dual active bridge (DAB) converter. From [3] it is found in general, when the voltage and current ratings of semiconductors are the same, the transmission power of the converter is proportional to the number of switches. This gives the DAB converter the advantage compared to several other similar topologies due to its eight switches. This converter normally operates with a phase shift modulation control. By utilizing a transformer with phase shifting the eight switches, a considerable voltage conversion ratio can be produced [3]. The DAB converter can also achieve soft switching using a series resonant circuit placed before the high-frequency transformer. To achieve this merit requires complex control using natural switching surface trajectories along with phase shift modulation techniques [4]. This converter is a suitable option for bidirectional capabilities that require a high voltage conversion ratio. However, if there is a need for a converter without a high-frequency transformer and a simple control technique that can achieve bidirectional power flow and soft switching, this converter is not the recommended option.

Another similar bidirectional dc-dc converter is the bidirectional buck-boost converter [5], [6]. This non-inverting four-switch converter has the ability to be bidirectional and achieve up to 97% efficiency in a 500 W system [7]. The converter is able to operate with fixed frequency using pseudo sliding mode control, which provides a robust controller and allows the converter to still achieve high efficiency in a dynamic environment [8]. This converter is extremely adaptable to low voltage systems that is connected to a varying DC bus. Although this converter can operate at high efficiencies and able to achieve bidirectional power flow, it would be challenging to make this circuit adaptable to medium or high voltage scenarios. This is

primarily due to the circuit's topology configuration that does not allow the voltage switching stress to be shared among multiple switches. In addition, without being able to achieve zero voltage switching, the longevity of the semiconductor switches could be lessened.

The AC-link design, shown in Figure 1.1, was based on the idea of a DC-link circuit. DC-link circuits are mainly used to couple two different circuits for one common voltage level. These circuits allow for a quick transfer of power, due to the high capacitance of the link capacitor. Additionally, another merit of these DC-links is the ability to transfer power even if large current spikes are present. However, creating an oscillating ac signal in the link permits the circuit to achieve soft switching thus increasing efficiency and improving the reliability and availability of the converter while keeping the added benefits of a circuit using a large dc electrolytic capacitor, but only having to use a less rated capacitor.

The dc-dc AC-link converter's main benefit is that it can achieve soft switching and has the capability to buck and boost the output voltage [9]. The AC-link topology is also referred to as "universal" because of its ability to achieve inputs and outputs as ac-ac, dc-ac, ac-dc, or dc-dc [2], [9], [10], given the correct topology. This power converter is able to achieve soft switching at the turn-on operation for each of its switches. This universal power converter can be considered state of the art for resonant converter designs and has been patented for its topology [1]. The AC-link topology is an extension of the buck-boost converter with the addition of a parallel resonant tank, which consist of a capacitor and an inductor. The inductor, being the main energy storage unit, resonates with the parallel capacitor to form a resonant circuit that will ensure soft switching for the converter. This idea of ensuring soft switching enables the buck-boost circuit to operate at high frequencies (~15 kHz or greater) with nearly negligible switching losses. Because of the versatility of this converter, it can be applied to a large variety of

applications. The input and output filters of this design are used to reduce voltage and current harmonics [11]. This converter also has the ability to have bidirectional power flow, and behaves similarly to the dual active bridge converter [12]. This crucial feature will allow the converter to operate in a wide range of dynamic voltage scenarios, such as connecting to a battery and to a fluctuating dc bus.

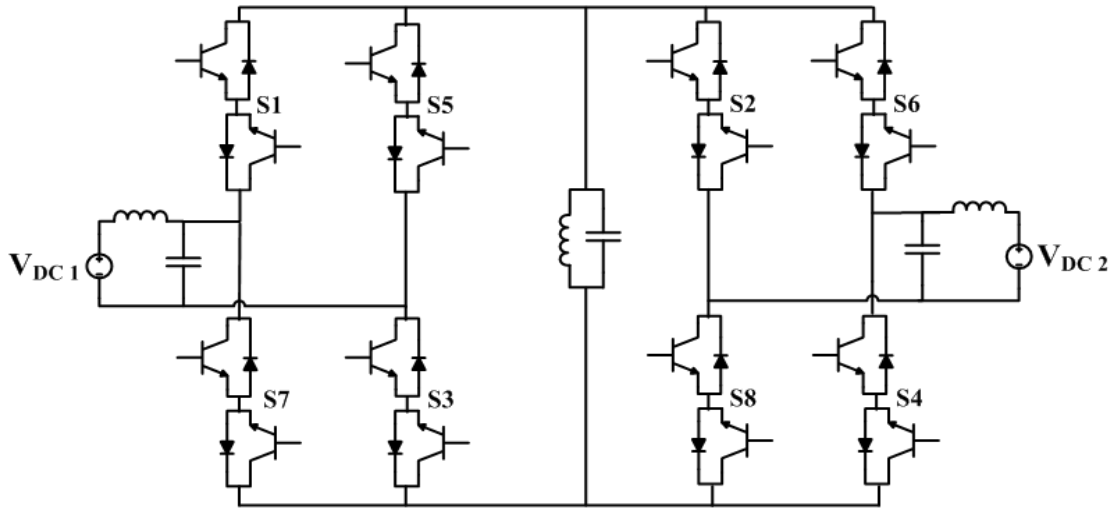


Figure 1:1 Bidirectional dc-dc AC-link topology [1]

The AC-link's resonant frequency is found by (1.1),

$$f_o = \frac{1}{2\pi\sqrt{L_r C_r}} \quad (1.1)$$

where L_r and C_r are the resonant tank's capacitor and inductor. A resonant frequency is the frequency in which the reactance of the capacitor equals the reactance of the inductor. The switching frequency is less than the resonant frequency, which is found approximately by combining the filters with the resonant tank and resolving for the frequency using (1.1).

This realization that the link current and inductor will be oscillating at a potentially high frequency mitigates the need for a large aluminum dc electrolytic capacitor within the link

because the smaller rated size of the capacitor the larger the resonant frequency will be [2]. The ability to reduce the overall capacitance of the converter, or to eliminate the need for electrolytic capacitors, is crucial for improving the reliability of the converter. This can be seen in Figure 1.2, where the comparison of aluminum electrolytic capacitors (Al-Caps), metallized polypropylene capacitors (MPPF-Caps), and high capacitance Multi-Layer Ceramic Capacitors (MLC-Caps) are shown [13].

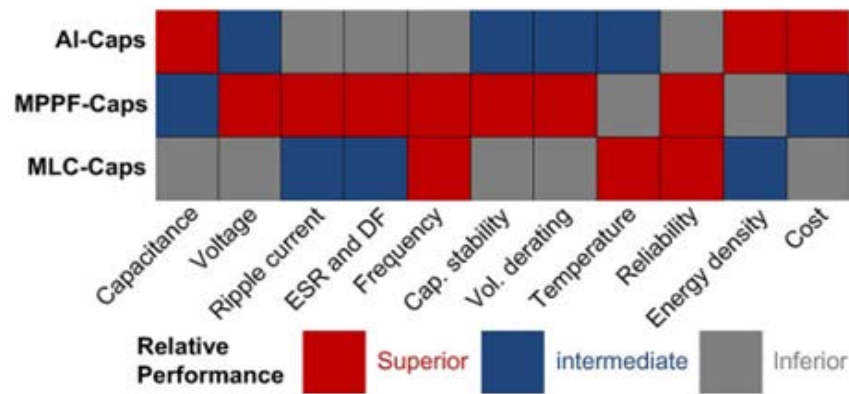


Figure 1.2: Evaluation of three common capacitors [13]

In Figure 1.2, it can be seen that the Al-Cap can achieve a very high capacitance and is cost effective; however, it has a very poor reliability and does not perform well at high frequencies. Thus, the AC-link topology is able to reduce the capacitance enough that the need for Al-Caps will become unnecessary and a more robust capacitor such as a MPPF or MLC capacitor can be used.

A popular way of lessening switching losses and improving reliability of power electronic devices is to introduce soft switching, or more specifically, zero voltage switching (ZVS) and/or zero current switching (ZCS). Soft switching, shown in Figure 1.3, is usually introduced through a type of resonant circuit, such as an inductor and capacitor (LC) circuit, and it takes place when the turn-on and turn-off of a semiconductor switching device overlaps with a

zero crossing of the voltage or current waveform [14]. In general, for this application the focus is on zero voltage switching.

In Figure 1.3, the red areas display the points in which loss, measured in watts, occurs when the semiconductor receives its gate input signal. In semiconductor switches like MOSFETs, soft switching typically eliminates the switching loss caused by diode recovery charge and the semiconductors parasitic capacitance. This is due to the diode recovery charge and semiconductor output capacitance being the major source of PWM switching losses [14]. Like MOSFETs, IGBTs can lose a significant amount of energy because of the current tailing phenomenon.

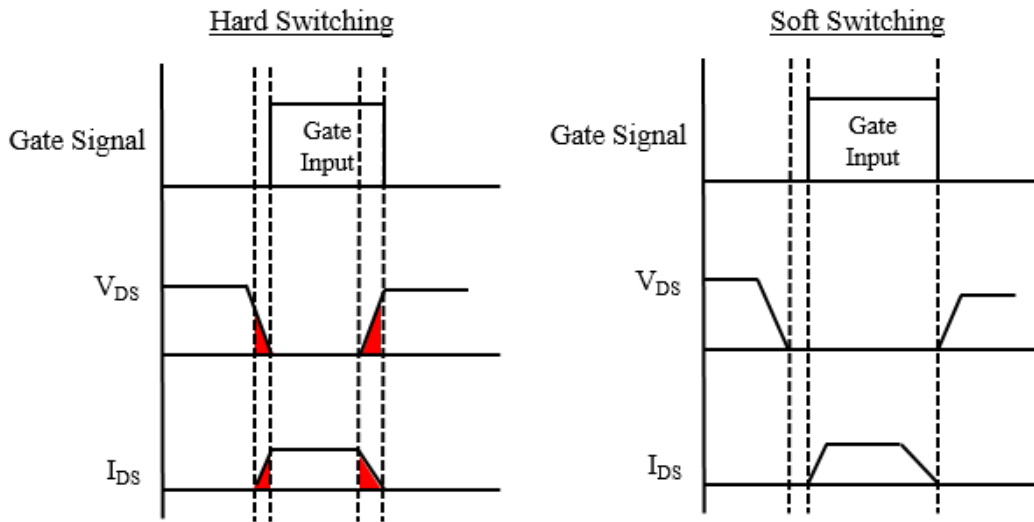


Figure 1:3: Hard switching vs soft switching in semiconductor

In a parallel LC tank design, zero voltage switching is investigated. In this type of design, if the switching frequency is less than the resonant frequency the tank will appear inductive. This will relate the current lagging the voltage and introduces the ability for the switch to turn on at a zero-voltage crossing, thus eliminating a major amount of loss. This concept of soft switching will be applied to this extension of a buck boost converter to reduce the amount of switching loss

created and allow the converter to operate at a higher switching frequency. Important equations for designing resonant systems are noted below [14].

$$X_L = 2\pi f_s L \quad (1.2)$$

$$X_C = \frac{1}{2\pi f_s C} \quad (1.3)$$

$$f_o = \frac{1}{2\pi\sqrt{LC}} \quad (1.4)$$

$$\omega_o = \frac{1}{\sqrt{LC}} \quad (1.5)$$

$$Z_o = \sqrt{\frac{L}{C}} \quad (1.6)$$

Here X_L is the inductive reactance, X_C is the capacitive reactance, f_o is the resonant frequency, ω_o is the angular frequency, and Z_o is the systems impedance at resonant frequency.

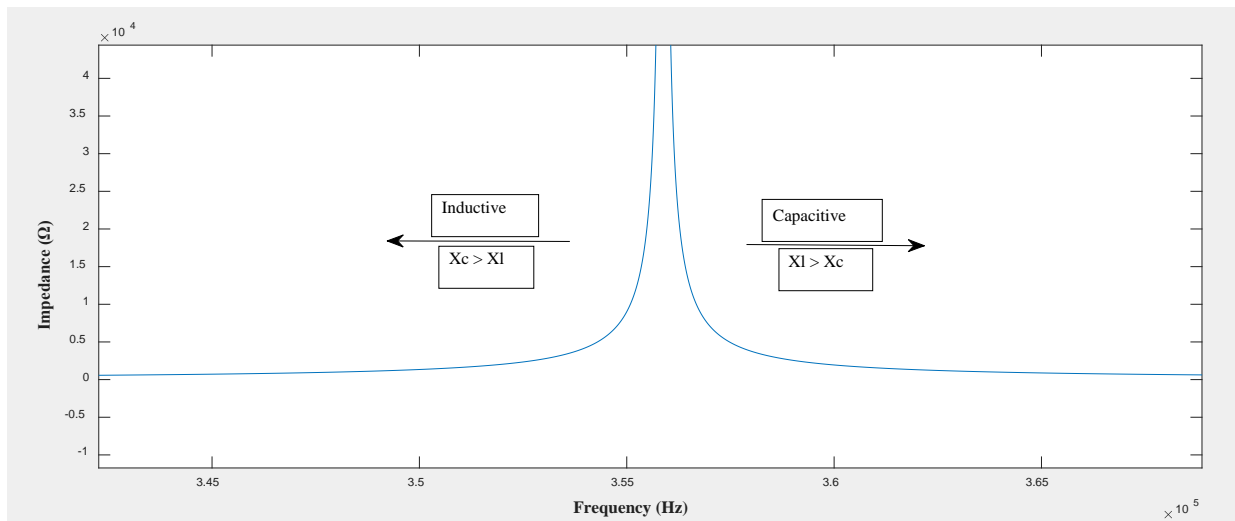


Figure 1:4: AC-link parallel resonant tank's characteristics at specific L and C values

The phenomenon for soft switching to occur happens from the resonant tank's characteristics, as seen in Figure 1.4. Again, to achieve zero voltage switching, the switching frequency of the circuit operates below the resonant frequency to create an inductive circuit, i.e. the current lags the voltage. This allows the switches to turn-on when the voltage is at a zero crossing and creates minimal losses for the device. This feature, along with a specific modulation, allows the converter to operate at reasonably high switching frequencies, which in turn can reduce the overall package of the device.

1.2 RESONANT CONTROLLER TECHNIQUES

Resonant circuits introduce many benefits for circuit operation from higher reliability to allowing operation at higher frequencies resulting in a more compact and smaller device. However, one of the most significant drawbacks of these types of circuits is the added complexity. This added complexity is due to the constant dynamic characteristics of parallel LC circuits. However, because of the merits of resonant topologies, extensive work has gone into the control, but focusing on series resonant topologies [15]. This led to the control techniques for series resonant tank converters which can be, but not limited to, frequency modulation control [15], energy feedback control [16], asymmetrical pulse width modulation [17], and sliding mode control [18]. However, even though these methods may work for a parallel resonant converter, control of the series resonant tank and parallel resonant tank still differ in a few ways.

The main difference between the series resonant tank, other than the configuration of the LC circuit, is that the parallel tank allows for a constant input current from the incoming voltage source. This feature allows for less current stress on the switches because the current is not

changing abruptly [15]. Also, in parallel resonant circuits, the reactive power is what circulates within the resonant tank and only the real power is provided through the semiconductor switches, which allows for the ability to produce high current and voltage levels using low rated volt-ampere switches and provides short circuit protection [15]. In this section, several popular control methods will be discussed on regulating the dynamic characteristics of parallel resonant tank circuits.

Frequency-modulation control (FMC) can be applied to parallel resonant circuits [15]. The idea behind this controller is similar to most, in that, it is used to regulate the output voltage and provide zero voltage switching for the circuit. This method is designed by creating the dynamic model of the open loop parallel circuit and obtain the small-signal model characteristics from the averaged model. The next step is to find the dynamic model for the closed loop system, which allow the control gains to be expressed. The actual frequency modulation (FM) portion of this controller is created by usually generating a saw-tooth waveform synchronized by the zero crossing detection of the resonant capacitor voltage [15]. It is then compared with the output signal of a controller in order to operate the corresponding switches. By combining this method with a proportional integral (PI) controller this method will allow for adaptability if components parameters change within the resonant tank, such as changes to the resonant tank's inductor or capacitor values varying over time. For instance, the frequency will increase if the tank begins to become overly inductive and the opposite for an overly capacitive circuit. This method is robust since it is adaptable to changes within the circuit; however, without the ability to be able to control the ever adapting switching frequency, damaging effects can be caused to the switches and other components within the device. Resonant circuits are very sensitive, especially when

using frequency control. Miniscule variations within the load or other parts of the converter can cause large current or voltage spikes, stressing electronics within the circuit [19].

Another method of controlling a parallel resonant converter is to use sliding-mode control [20]. This method operates with amplitude modulation, which leads to a robust form of control. The sliding-mode control is adaptable for transient prone systems and also systems that will obtain component value variations [21]. This method's switching frequency acclimatizes automatically to fluctuations of component values while still preserving soft switching conditions. The control of this system uses feedforward control, which is a major contributor to why this system can adapt to abrupt load shifts. The main idea of this converter is to maintain the operation of the converter on the switching surface by developing multiple threshold values. Sliding mode control can be a simple method of controlling a converter, however, in this case with the AC-link converter, implementing this control would be rather complex. The complexity of this control comes from the many modes of the controller and the number of switches that need to be regulated. Developing the phase trajectory is very tedious, and can be extremely difficult in higher order systems like the AC-link topology [22].

An additional method for controlling a parallel resonant circuit is to use a linear controller with fixed frequency control. This method uses a PI controller and analog control gates to regulate the input gate signal of the switches [9]. Analog control has a fast response time and is usually less costly than digital controllers like field programmable gate arrays (FPGA). This constant switching frequency method measures voltages and currents throughout the circuit to compare polarities of what the expected voltages and currents should be. By monitoring the state of the voltages and currents, the switches can achieve soft switching by allowing a zero potential difference between switches during different modes of operation [9]. With an

equilibrium voltage point on each side of a switch, the voltage across the switch at turn-on is zero. This is the general way of obtaining zero voltage switching (ZVS). However, this method does not handle the dynamics of the resonant circuit as well as would be desired. The resonating cycle of the parallel LC circuit oscillates rapidly. Using a fixed frequency control method while measuring the polarities of the resonant tank's voltage and current and comparing those values to the voltages and currents on the filters, issues may arise such as incorrect gate signals being sent to trigger the semiconductors.

The sensitivity of resonant circuit design led to the development of control methods depending upon state variable regulation within the resonant circuit. One of the first discoveries of implementing a state variable regulation controller is found in [23] where the term optimal trajectory control (OTC) originated. The OTC method shows a much better dynamic performance than just using linear control methods. This is due to the immediate transfer between operating points by using comparative techniques with voltage and current states measured continuously throughout the operation of the converter [24]. The control proposed within this work, state plane trajectory control (SPTC), is a method based on OTC without deriving the precise optimal trajectories for the various modes of a circuit. The idea of monitoring the state variables values (capacitor voltage and inductor current) to follow a desired set reference trajectory is beneficial for effectively eliminating unwanted over voltages and over currents. This creates near instantaneous transition between operating modes that would occur for load changes or other transient events. Adaptation of SPTC for parallel resonant circuits simply requires the dynamic resonant equations from the equivalent switching circuits to measure the radius of each trajectory for each corresponding mode.

This method uses a point-by-point control scheme that allows the converter to operate at its own resonant frequency. This method does not force artificial switching signals and can still achieve soft switched bidirectional power flow. The SPTC can adapt to load variations rapidly due to its instantaneous properties, similar to OTC. In Figure 1.5, an example of SPTC is shown. State plane analysis and normalization will be discussed in the next section of this document. However, the basis of this control method is to continuously measure the current and voltage within the resonant tank and compare those values to reference values, which are predetermined. For example, R1a will start conducting at a certain current reference then follow the trajectory and conclude at R1b reaches a voltage reference. This control method will be further explained in upcoming sections.

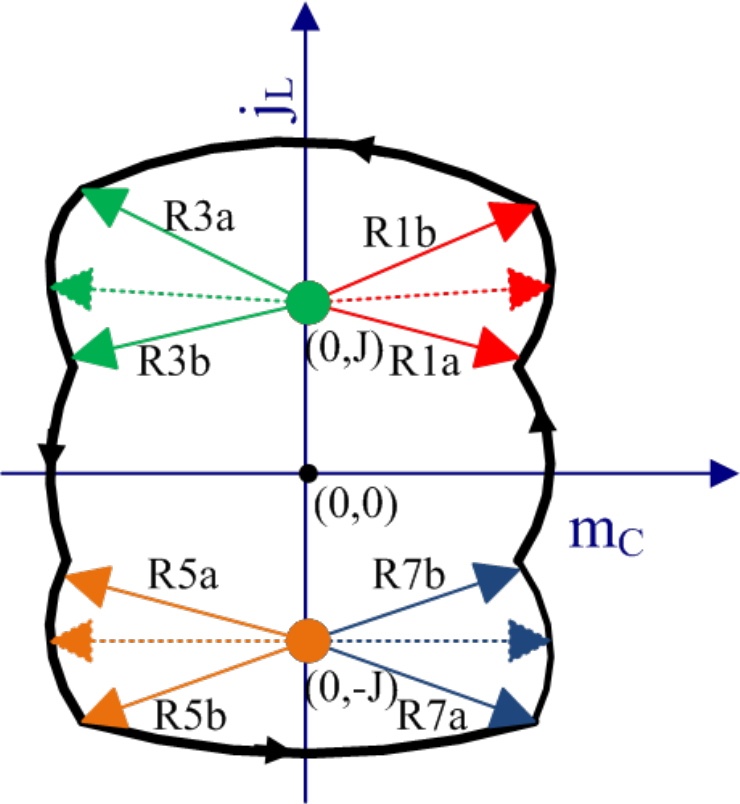


Figure 1:5: Example of SPTC on normalized current vs voltage plot with 1:1 voltage transfer

2.0 STATE PLANE TRAJECTORY

The AC-link universal power converter can be considered state of the art for resonant converter designs. However, a comprehensive mathematical analysis for this structure is lacking and is provided in this work.

For a pulse width modulation (PWM) controller, the state-space average method can be applied without inaccuracies when analyzing a converter. In addition, small signal models can be used to describe the dynamics of the system, but they only operate at a single operating point, so that method is not a comprehensive when dealing with transient events for an analysis standpoint. The average modeling method does not work, as well, for resonant tanks because this method will effectively remove information associated with the switching frequency. This means the dynamic characteristics of the tank will also be lost [24]. However, state-plane analysis can be used to understand the dynamic behavior of the parallel resonant tank. State plane trajectory methods are applied to circuits such as resonate tank circuits because the switching frequency will be close to the resonant frequency [24].

State-plane analysis ensures a very good understanding of dynamics and steady state characteristics of a resonant tank [25]. The state-plane analysis method takes less computational power than the simulation based method, extended described function, and multi frequency averaging [25]. In addition, besides the long computation, the mentioned control methods operate around a single operating point, which means they do not function properly in load

variation, or transient events. The graphical state plane of the resonating tank is a clear and informational tool that can represent the different states of the operation of the converter. From the benefits mentioned about using state plane analysis when observing a resonant converter, the clear method of controlling a converter when using state plane analysis is to use the optimal trajectory control or similar method.

State plane trajectories display the normalized current and voltage for two state variables within the equivalent circuits of each mode. This means when creating the equivalent circuits there can only be one inductor and one capacitor because the state-plane trajectory can only be simply implemented on a two-dimensional plane [24]. Theoretically, the state plane can be three-dimensional; however, this creates a much more complicated analysis. Normalization of the switching mode equations significantly simplifies the geometric analysis of the state plane trajectories by utilizing the characteristic impedance and base voltage conversions, shown in Table 1. This creates a unit less chart (similar to per unit method for power systems) to have a clearer analysis of the resonant circuit.

For ease of analysis, the input and output filter inductors are assumed large enough to behave as current sources. Additionally, in order to avoid 3-dimensional trajectory analysis due to three energy storage elements (state variables) in the circuit in any given mode of operation, the resonant tank capacitance in parallel with the filter capacitance ($C_{fx} // C_r$) will be considered as an equivalent network capacitance. With these assumptions, Figure 1.1 operates in eight modes to be explained in the forthcoming sections. The center of the state plane trajectory for each mode is found by determining the steady state dc value of the corresponding equivalent circuit.

Table 1: Normalization Conversion Chart

Parameter	Conversion
Base Voltage (V)	V_{in}
Normalized Resonant Capacitor Voltage	$m = \frac{v_c}{V_{base}}$
Normalized Load Voltage	$M = \frac{V}{V_{base}}$
Base Current (A)	$I_{base} = \frac{V_{base}}{R_o}$
Normalized Resonant Inductor Current	$j = \frac{i_L}{I_{base}}$
Normalized Load Current	$I = \frac{I}{I_{base}}$
Characteristic Impedance (Ω)	$R_o = \sqrt{\frac{L_r}{C_r}}$
Tank Resonant Angular Frequency (<i>rad/s</i>)	$\omega_0 = \frac{1}{\sqrt{L_r C_r}}$
Angle in Trajectory (rad)	$\theta = \omega_0 t$

2.1 EQUIVALENT CIRCUITS FOR DC-DC AC-LINK CONVERTER

To identify the ideal trajectories for this converter and visually explain the dynamics of the resonant tank, the state plane analysis method can be utilized [26]. This method looks at the equivalent circuit for each mode of operation to determine its natural voltage and current trajectory in a normalized form. The geometric analysis of the state plane trajectories are simplified significantly after normalizing the equations for each mode by a base impedance and base voltage. The conversions for the normalization are shown in Table 1. This involves solving for the equivalent circuits for each anticipated mode of operation for the converter. By solving these circuits, the voltage, current, and impedance can be normalized to develop the graphical state-plane trajectory tool. The circuits are solved by simply finding the voltage across the capacitor and current through the inductor in the AC-link.

In order to solve for the state plane trajectory, there needs to be two state variables, which require the combination of capacitance from the input filter capacitor and the resonant capacitor for modes 1 and 5 and the combination of the output filter capacitor and the resonant capacitor for modes 3 and 7. The input and output filter inductors are large enough (much greater than resonant inductor) to be treated as a current source. For the sake of simplicity and avoiding redundancy, mode 1 (Figure 2.1 and Figure 2.2), mode 2 (Figure 2.3 and Figure 2.4), and mode 7 (Figure 2.5 and Figure 2.6) are only shown to display the different trajectories.

2.1.1 Mode 1 – Charging with Positive Polarity

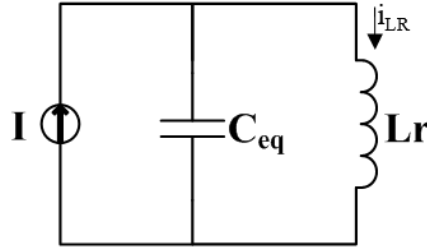


Figure 2:1: Equivalent circuit for mode 1

$$L_r \frac{di}{dt} = V_{Ci} \quad (2.1)$$

$$C_{eq} \frac{dv}{dt} = I_{in} - i_{Lr} \quad (2.2)$$

Here V_{Ci} is the voltage across the input filter capacitor combined with the resonant tank capacitor and i_{Lr} is the current through the resonant tank inductor.

After deriving the voltage across the capacitor and current through the inductor, the following equations can be realized after normalizing the parameters from using Table 1.

$$\frac{dj}{d\theta} = m \quad (2.3)$$

$$\frac{dm}{d\theta} = J - j \quad (2.4)$$

$$A = \sqrt{M_o^2 + (J_o - J)^2} \quad (2.5)$$

Where A is the radius of the trajectory from the initial conditions regarding mode 1 and M_o and J_o are the initial normalized voltage and current within the variables.

$$m(\theta) = A \cos(\theta + \theta_0) \quad (2.6)$$

$$j(\theta) = -J + A \sin(\theta + \theta_0) \quad (2.7)$$

$$\tan(\theta_0) = \frac{-J + J_0}{M_0} \quad (2.8)$$

Where $m(\theta)$ and $j(\theta)$ are the solutions of the second-order system of linear differential equations.

It can be noticed that the normalized current solution contains a dc term and both solutions contain a sinusoidal term that represents the ac ringing response of the tank.

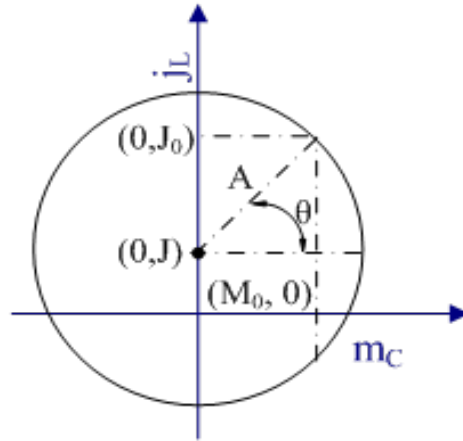


Figure 2:2: State plane trajectory for mode 1

The center of the state plane trajectory for all of the modes are found by recognizing the dc steady state value of the equivalent circuit. The solutions provided above describe a circle in a normalized state plane. Figure 2.2, Figure 2.4, and Figure 2.6 are undamped, as the solutions are derived in ideal conditions. The diameter and radius of the circles are dependent on the initial conditions of the current and voltage within the LC circuit.

2.1.2 Mode 2, 4, 6, and 8 – Resonance

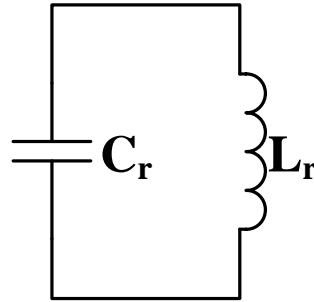


Figure 2:3: Equivalent circuit for mode 2

$$L_r \frac{di}{dt} = V_{C_r} \quad (2.9)$$

$$C_r \frac{dv}{dt} = i_{L_r} \quad (2.10)$$

Where V_{C_r} is the voltage across the resonant tank capacitor and i_{L_r} is the current through the resonant tank inductor.

After deriving the voltage across the capacitor and current through the inductor, the following equations can be realized after normalizing the parameters from using Table 1.

$$\frac{dj}{d\theta} = m \quad (2.11)$$

$$\frac{dm}{d\theta} = j \quad (2.12)$$

$$A = \sqrt{M_o^2 + J_o^2} \quad (2.13)$$

Where A is the radius of the trajectory from the initial conditions regarding mode 1 and M_0 and J_0 are the initial normalized voltage and current within the variables.

$$m(\theta) = A \cos(\theta + \theta_0) \quad (2.14)$$

$$j(\theta) = A \sin(\theta + \theta_0) \quad (2.15)$$

$$\tan(\theta_0) = \frac{J_0}{M_0} \quad (2.16)$$

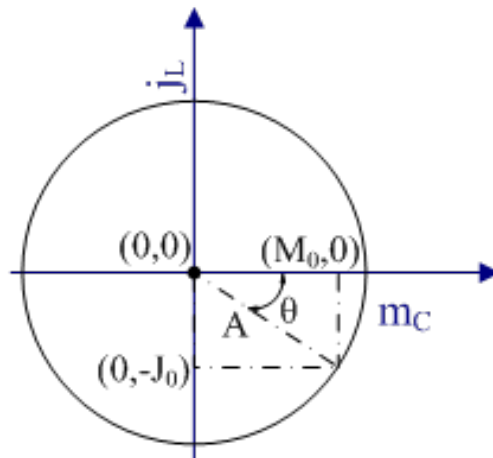


Figure 2:4: State plane trajectory for mode 2

2.1.3 Mode 7 – Discharging with Negative Polarity

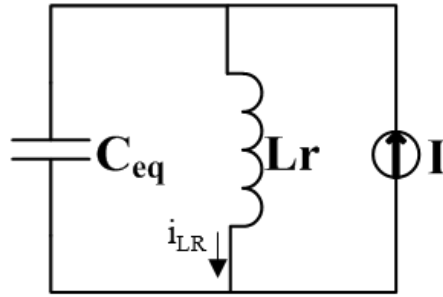


Figure 2:5: Equivalent circuit for mode 7

$$L_r \frac{di}{dt} = V_{C_{co}} \quad (2.17)$$

$$C_{eq} \frac{dv}{dt} = i_{L_r} - I_{out} \quad (2.18)$$

Where $V_{C_{co}}$ is the voltage across the output filter capacitor combined with the resonant tank capacitor and i_{L_r} is the current through the resonant tank inductor.

After deriving the voltage across the capacitor and current through the inductor, the following equations can be realized after normalizing the parameters from using Table 1.

$$\frac{dj}{d\theta} = m \quad (2.19)$$

$$\frac{dm}{d\theta} = j - J \quad (2.20)$$

$$A = \sqrt{M_o^2 + (J_o + J)^2} \quad (2.21)$$

Where A is the radius of the trajectory from the initial conditions regarding mode 1 and M_0 and J_0 are the initial normalized voltage and current within the variables.

$$m(\theta) = A \cos(\theta + \theta_0) \quad (2.22)$$

$$j(\theta) = J - A \sin(\theta + \theta_0) \quad (2.23)$$

$$\tan(\theta_0) = \frac{J - J_0}{M_0} \quad (2.24)$$

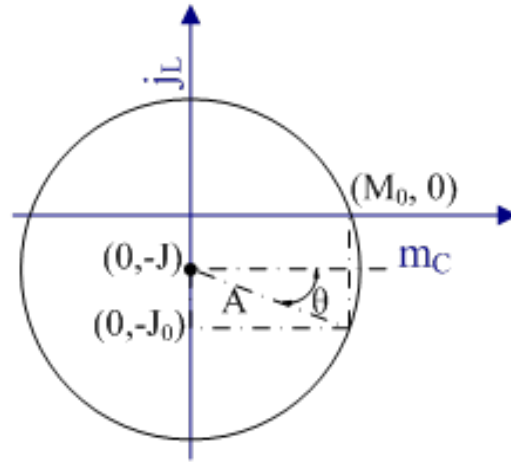


Figure 2:6: State plane trajectory for mode 7

3.0 OPERATION OF DC-DC AC-LINK CONVERTER

To obtain a deeper understanding of the behavior for the dc-dc AC-link converter, a visual aid for the modes of the circuit can be created for the LC tank within the converter. In order to create both positive and negative current directions, the switches must be organized in a specific order. This allows for a variation of the flow of currents to create oscillations within the resonant tank to institute ac-like characteristics.

The following images, Figure 3.1 and Figure 3.2, display the resonant tanks voltage and current during operation.

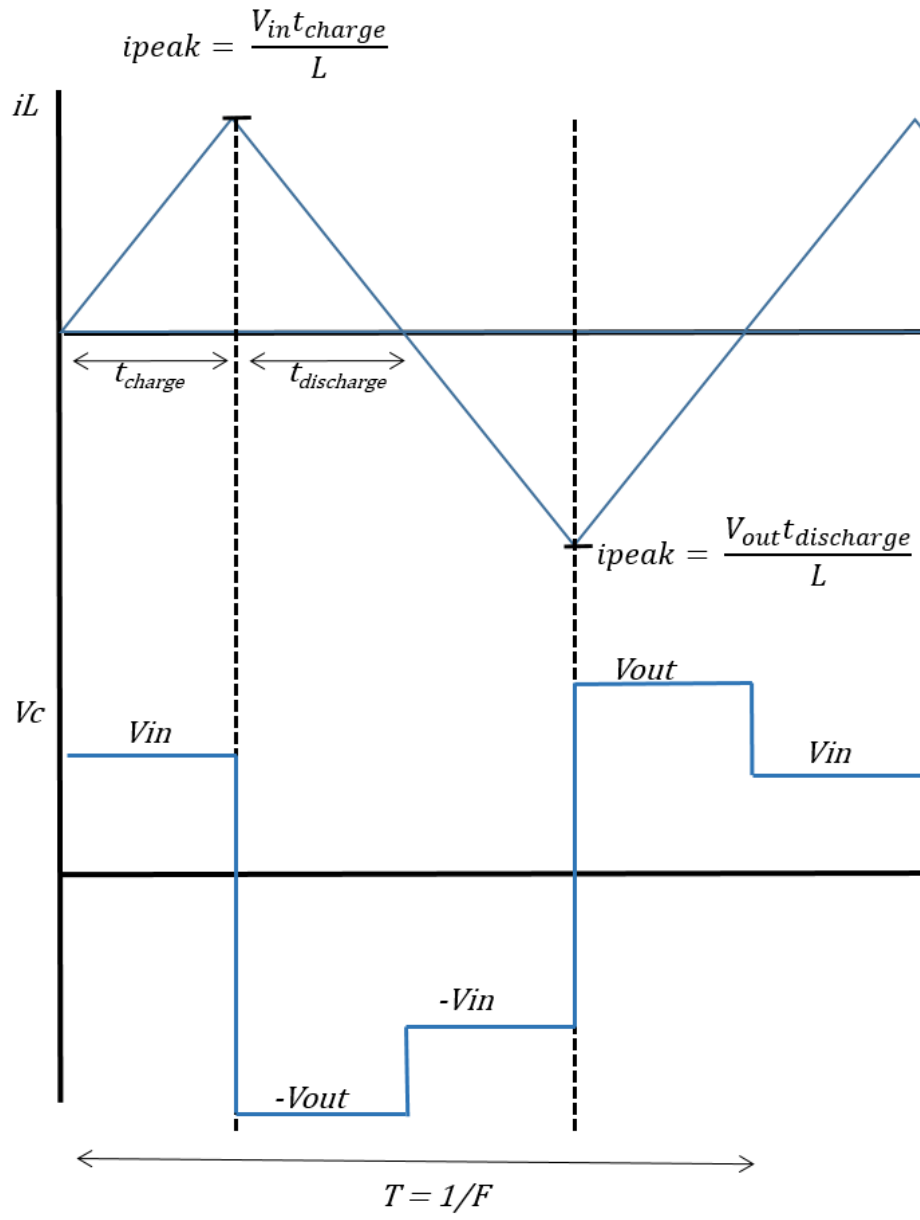


Figure 3:1: Theoretical output at AC-link converter neglecting resonant modes [2]

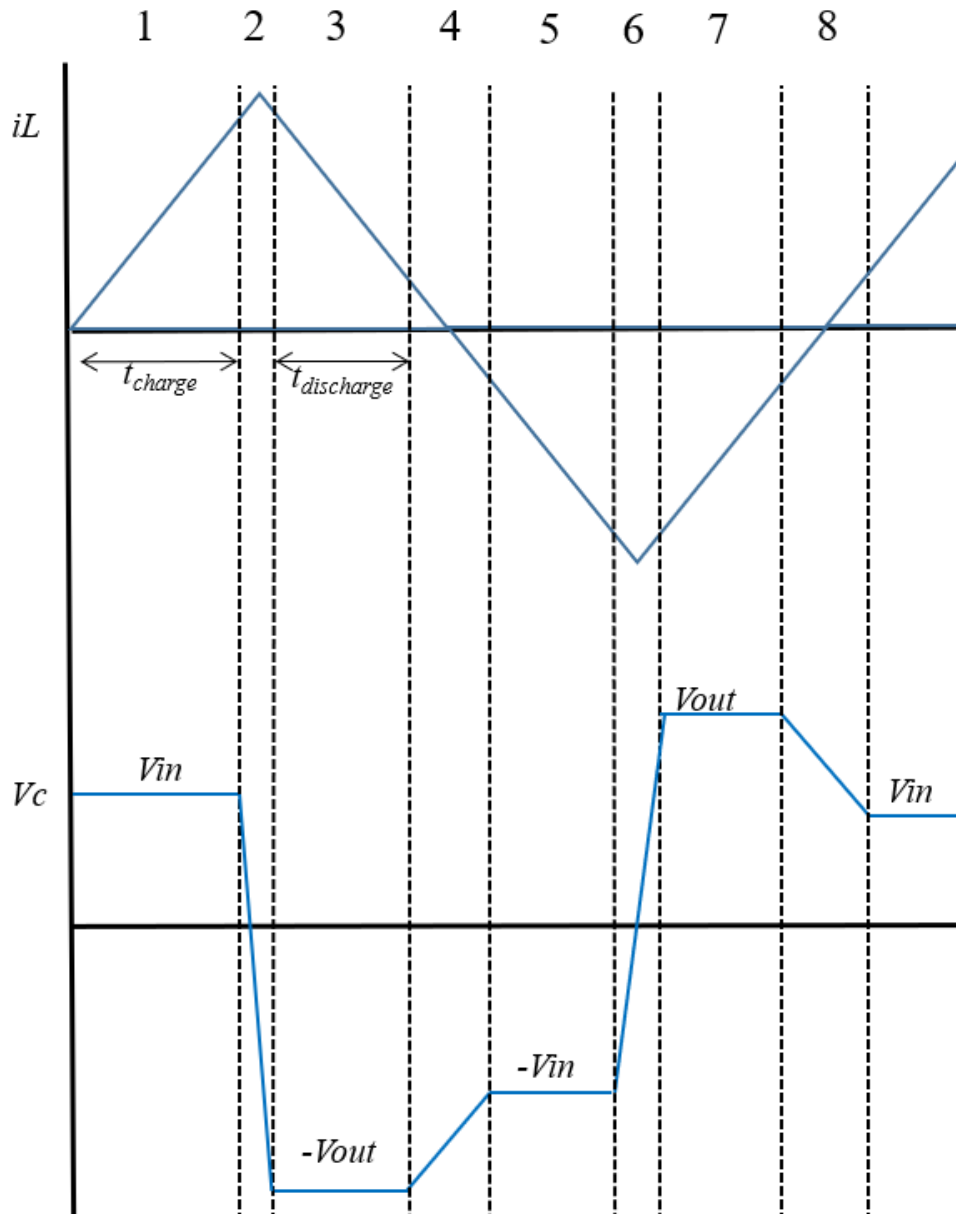


Figure 3.2: Theoretical output at AC-link with resonant modes in boost mode [2]

In Figure 3.2, the theoretical output of the converter is shown. The modes of the converters operation are displayed in the top of the figure labeled 1 through 8. The figure displays the waveforms of the voltage across the capacitor and current through the inductor in the resonant tank. An important characteristic to note is the ac-like features of the current in the tank. This is what facilitates the ZVS in the converter. ZVS for this circuit will occur by

permitting the resonant tank to naturally oscillate from the charged voltage to the same voltage on the opposite end of the semiconductor switch. By having the same potential voltage on each side of the switch, essentially the switch will turn on with a zero voltage potential difference. In addition, it is important to mention when the converter is resonating from mode to mode, the voltage will rapidly increase or decrease to meet either source 1's or source 2's voltage. This feature permits the switches to close when the voltage is equivalent at the link and at the connecting source's voltage, effectively having zero voltage potential difference. However, not shown in Figure 3.2, the voltage will have a V_{\max} value when transitioning from the odd number of modes, or from the resonant mode to the next mode. This occurs because when the converter resonates, a slight overshoot of voltage will occur in order to reach the desired source's voltage.

In Figure 3.1 and Figure 3.2, it can be seen that the current linearly charges and discharges. Figure 3.2 displays the expected behavior of the circuit while including the resonant modes. These modes allow the soft switching action to take place during the transition between power transfer modes, i.e. odd number modes, as mentioned earlier. Typically, the resonating time occurs so rapidly it can be neglected, but for a detailed analysis it is recommended to still solve for the peak current and voltage [2], [15]. This is found by (2.25) and (2.26).

$$I_{linkpeak_pos} = \frac{V_{in} t_{charge}}{L} \quad (2.25)$$

$$I_{linkpeak_neg} = \frac{V_{out} t_{discharge}}{L} \quad (2.26)$$

To analytically predict the peak voltage for the resonant circuit in the even number of modes, (2.27) can be used.

$$v(t) = I_o Z_o \sin(\omega_o t) + V_o \cos(\omega_o t) \quad (2.27)$$

Here I_o and V_o are the initial conditions and Z_o is the characteristic resistance.

3.1 BEHAVIOR OF AC-LINK CONVERTER IN DIFFERENT MODES WITH TRAJECTORIES

To further the analysis on the dc-dc AC-link converter, graphical models for the modes of the circuit with each associated trajectories, all for *buck* operation of the converter, are displayed in Figure 3.3, Figure 3.4, and Figure 3.5. In order to create both positive and negative current directions the switches must be organized to allow a variation of the flow of currents to create an oscillation within the resonant tank.

A. Mode 1

The first mode of operation for the dc-dc AC-link converter is to charge the resonant tank to a specified current reference. This mode is initiated by turning on switches $S1$ and $S3$ until the link voltage equals the input voltage to allow for zero voltage switching (ZVS).

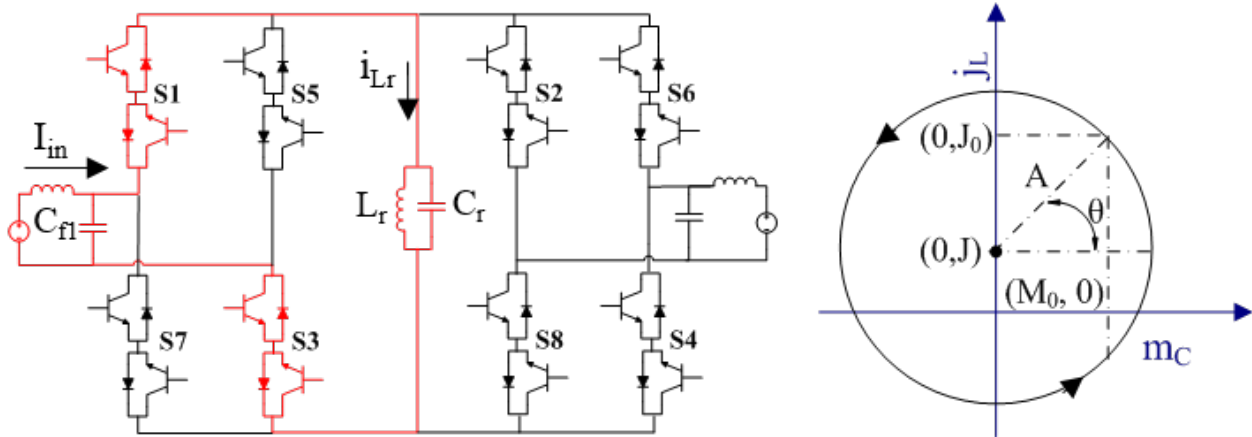


Figure 3:3: Operation of mode 1 with corresponding trajectory

B. Modes 2, 4, 6, & 8

The even numbered modes correspond to the resonating state of the converter. During these modes, no switches conduct, and the LC tank oscillates passing the energy back and forth from the inductor to the capacitor. These interim modes facilitate the ZVS characteristics for the converter because the switches delay conduction until the link voltage matches the desired voltage reference, whether mode transitioning from charging to discharging or vice versa.

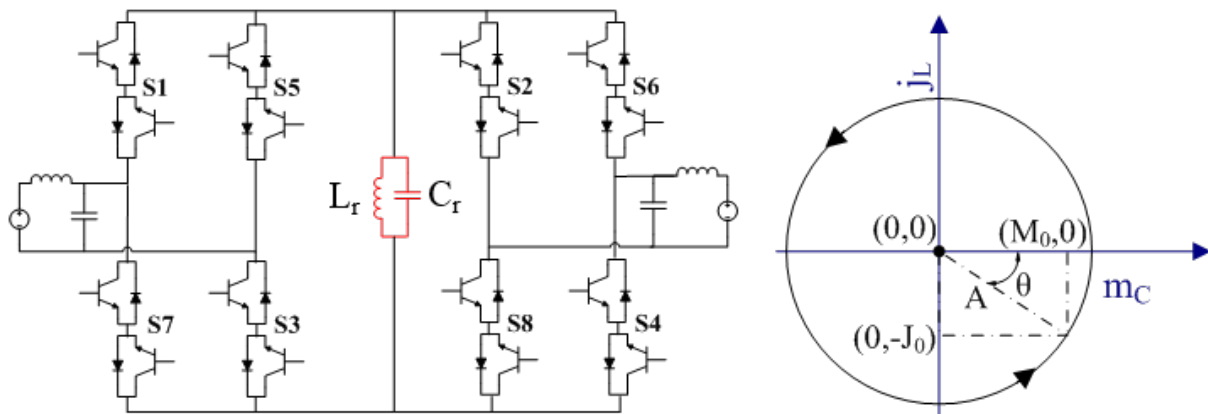


Figure 3:4: Operation of modes 2, 4, 6, and 8 with corresponding trajectory

C. Mode 7

During the seventh mode, the energy stored in the resonant tank is discharged to the output. This mode is initiated once the link voltage reaches the desired reference output voltage. This enables zero voltage switching because the voltage potential between the equivalent circuit at the resonant tank and the equivalent circuit at the output side is zero. Switches $S6$ and $S8$ close until the output current reaches its reference value. The reference current value ensures enough power is transferred from the resonant tank to the output source. This also allows the natural trajectory of the tank to switch from its previous positive polarity to a negative polarity to permit the desired operation of the AC-link.

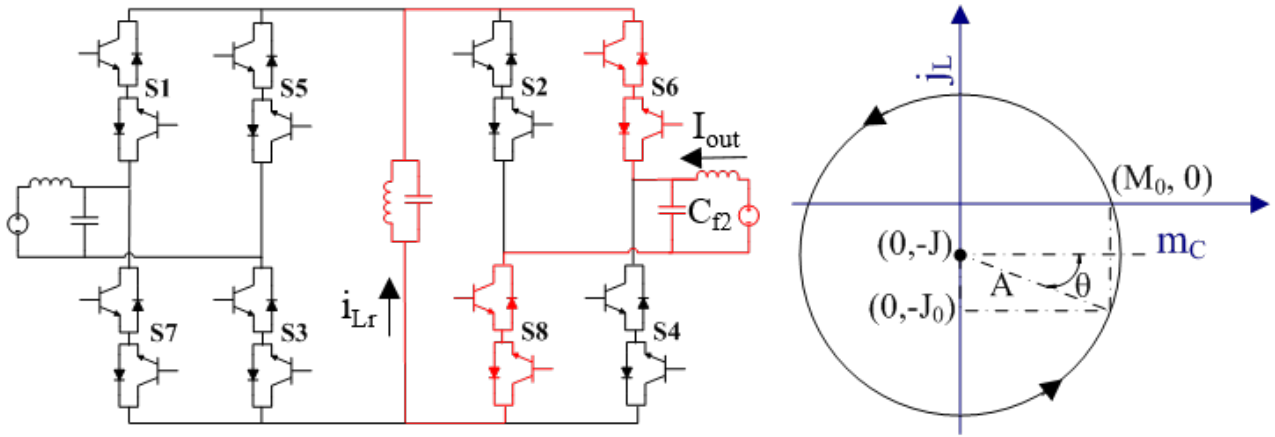


Figure 3:5: Operation of mode 7 with corresponding trajectory

D. Mode 3 & 5

Mode 5 is similar to mode 1 with the same equivalent circuit, except during this operation the current flows in the opposite direction by activating switches $S5$ and $S7$. This lets the resonant tank charge in a negative direction, which allows the tank to acquire AC current characteristics. Mode 3 is similar to mode 7, except

this mode permits the tank to discharge its current with a positive current by activating switches S_2 and S_4 . This will also allow AC characteristics to generate within the resonant tank, ultimately facilitating zero voltage switching.

4.0 STATE PLANE TRAJECTORY SWITCHING SEQUENCE

To properly control the transitions between the modes given in section 3.1, state plane trajectory control (SPTC) is utilized. The state plane analysis approach taken in this work is related to [27] where this method is applied to control a dual active bridge converter. This control technique, inspired from OTC, utilizes the natural resonance frequency generated by the LC tank for the converter to operate around specified coordinates, following a desired trajectory. Figure 4.1 and Figure 4.2 provides a theoretical graphical state plane trajectory showing the normalized voltage against the normalized current for all of the described modes combined into one full switching cycle bucking or boosting the voltage. Each mode corresponds to a given radius (R_{nx}). For example, mode 1 begins at $R1a$ when the link voltage equals the input voltage and ends at the tip of $R1b$ when the link current reaches its desired reference. The converter will then resonate to the tip of $R3a$ following the large outer half circle reaching the negative value of the desired output voltage value. The peak value of the outer circle can be solved using 2.27.

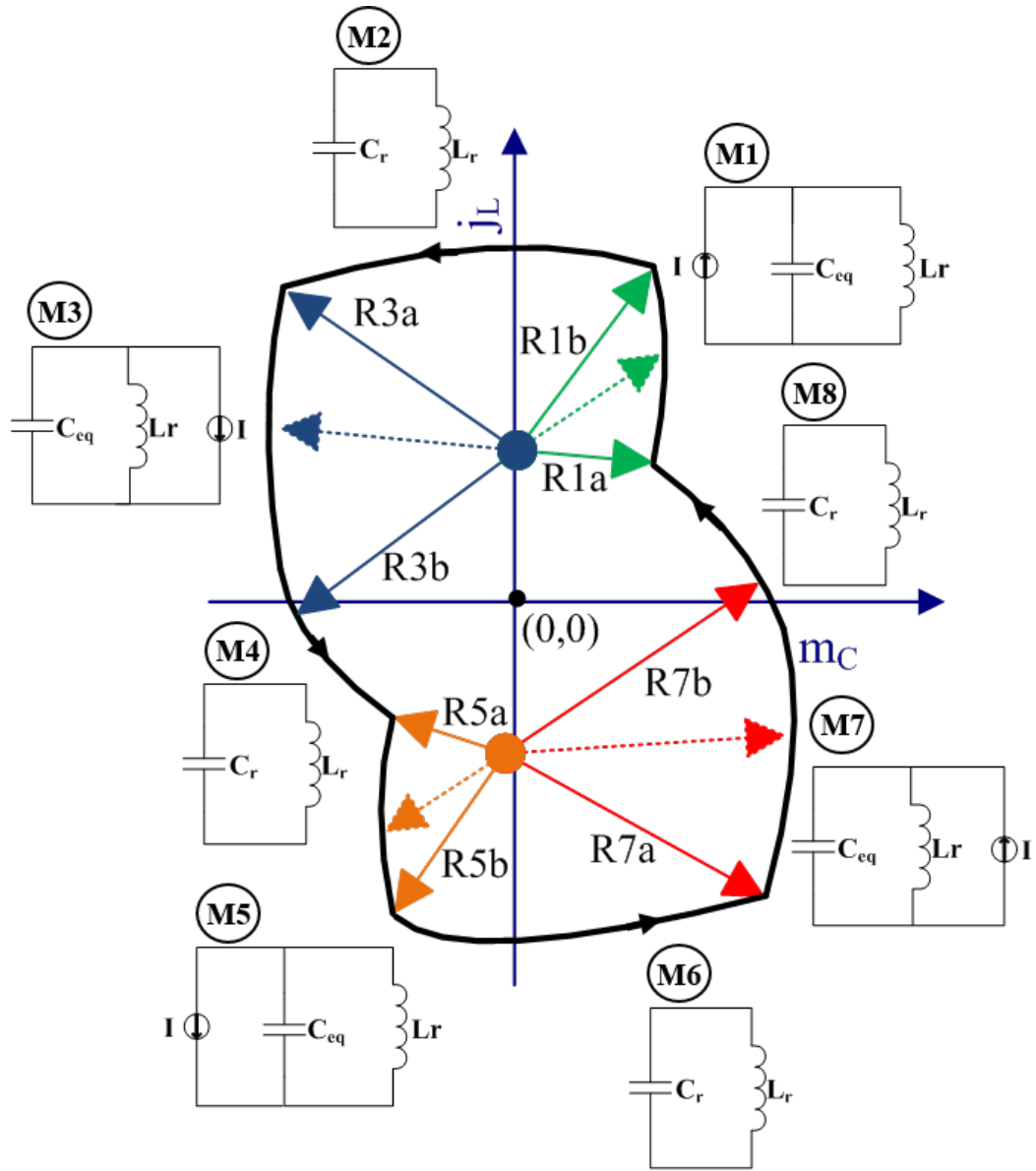


Figure 4:1: Theoretical combined state plane trajectory during boost mode of operation

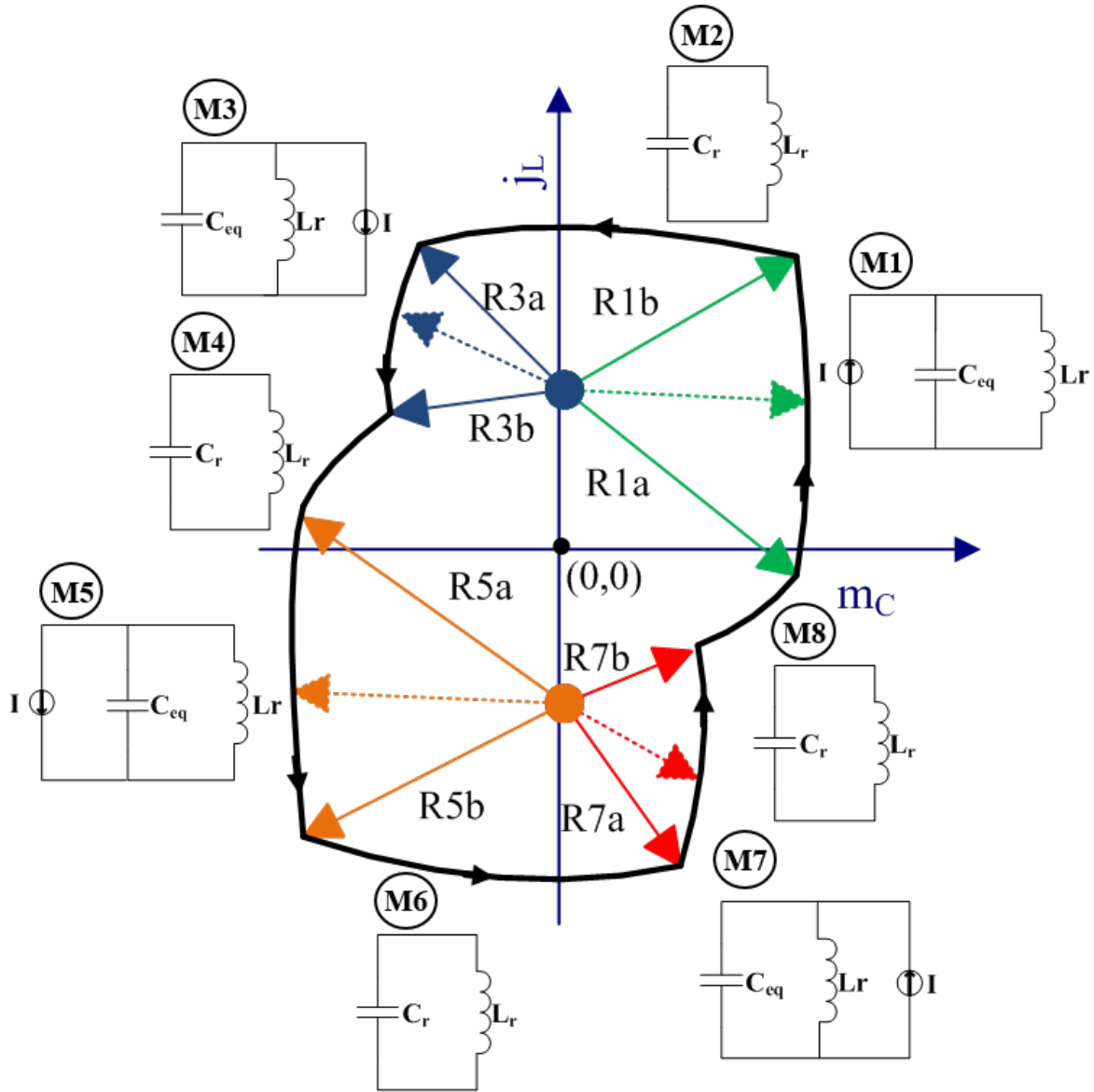


Figure 4:2: Theoretical combined state plane trajectory during buck mode of operation

In reference to Figure 4.1 and Figure 4.2, the system will operate counter clockwise. The resonant tank charge modes, 1 and 5, will have a slight curvature because the inductive load of the tank is being charged in each case. After the tank is charged, either mode 2 or 6 occurs respectively, where the converter tank will resonate. This is represented by the larger outer half circle in figures. The discharging modes, 3 and 7, will appear linear because the energy stored within the resonant tank will merely discharge into an infinite bus (source). The middle half

circle, modes 4 and 8, corresponds to resonant modes for when the system is transitioning from the discharge modes to the charging modes. The tank, at this point, has less power and therefore lowers its initial conditions that reduces the size of the trajectory. This converter can operate both voltage step-up and step-down conversions, similar to the dual active bridge converter.

4.1 SWITCH SEQUENCE LOGIC

A state machine, as shown in Figure 4.3, was programmed in PLECS by incorporating the logic design as demonstrated in the sequence diagram in Figure 4.4. The control block senses the desired direction of power flow, reference voltage, PI controlled link reference current, link voltage, link current, and both source voltages. Once each condition to trigger the next mode of operation is met, the gate signals associated with that next mode are then sent to the correct set of switches.

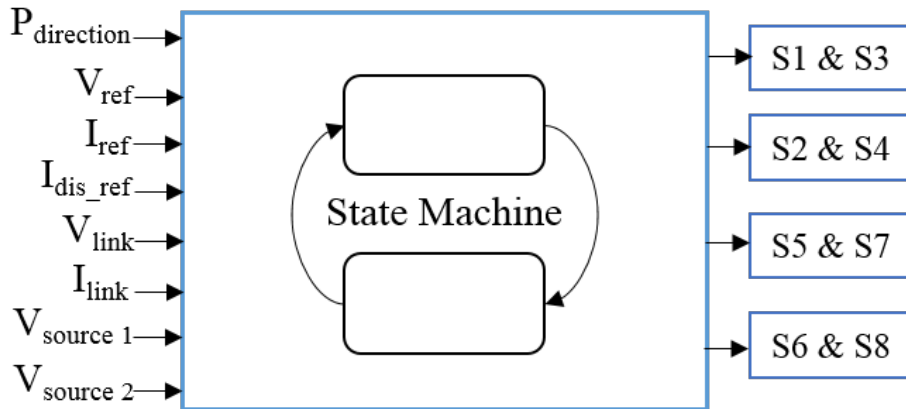


Figure 4.3: State machine for SPTC for AC-Link converter

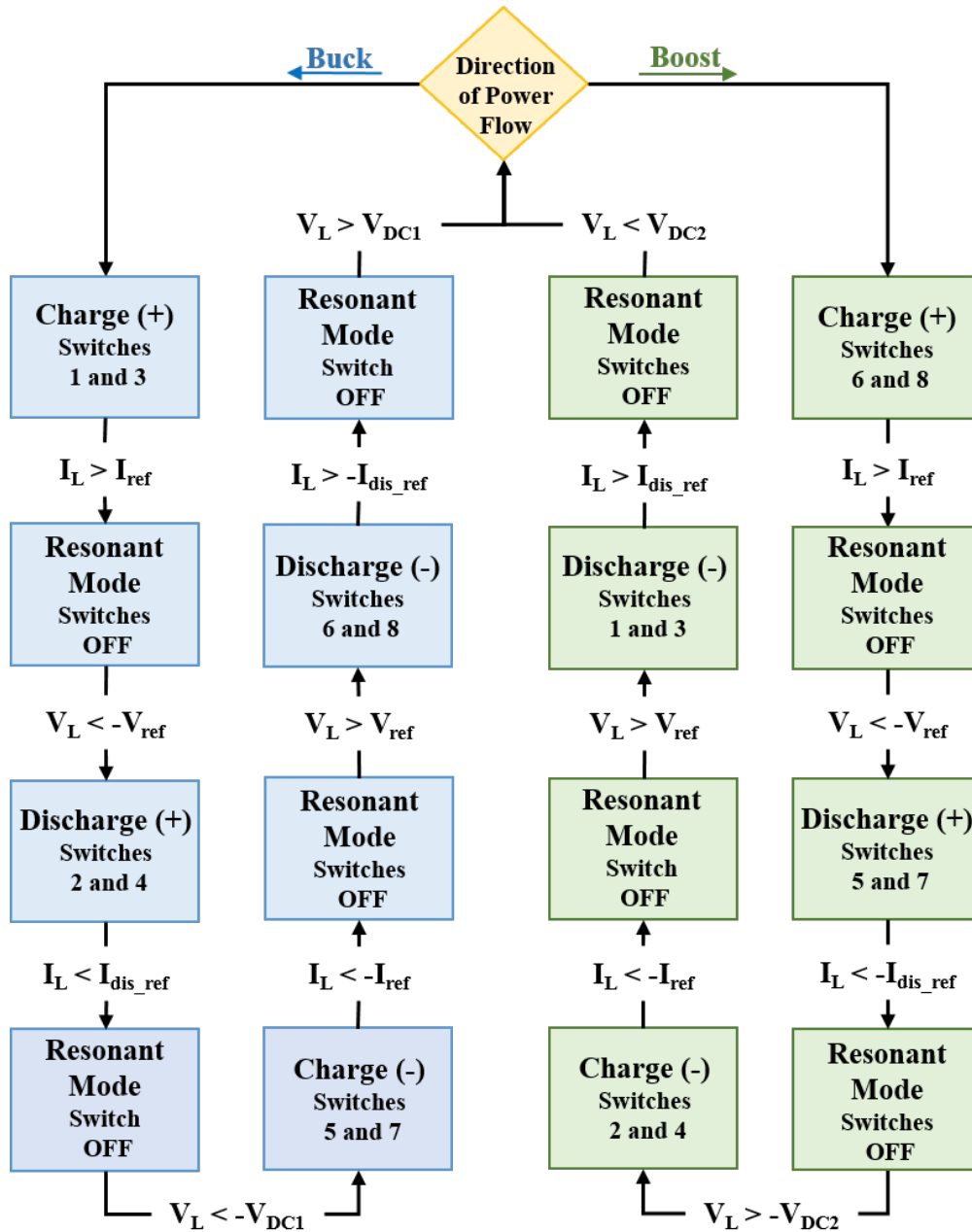


Figure 4:4: System logic for buck and boost modes of operation for state machine controller

To fully explain Figure 4.4, a systematic procedure of operations will be discussed. The *boost mode* is explained here. First, the logic senses which direction the user wants the power to flow by toggling a numerical value. Once the state machine recognizes it is sending power from source 2 (right side in Figure 1.1) to source 1 (left), it will begin to charge the resonant tank in a

positive current direction by switching on IGBTs $S6$ and $S8$. The resonant tank's current value will begin to increase linearly while the voltage remains equal to the secondary source. Once the current reaches its target, I_{ref} , it transitions to a resonating mode where no switches are closed. I_{ref} is chosen based upon the power rating of the converter. Then the actual power is calculated at the terminals of the absorbing end of the converter; in the boost case, source 1 is absorbing energy.

The converter will stay in the resonant state until the link voltage equals the reference voltage. This reference voltage is either source 1 or source 2 voltage, depending upon whether in buck or boost mode respectively. In boost mode, the reference voltage is source 1. The reasoning for this is to allow the switches on source 1's side to be the same voltage across the AC-link. This permits ZVS by letting the potential voltage between the AC-link and the filters on source 1 to be zero. Once the AC-link voltage reaches source 1's voltage level, IGBTs $S5$ and $S7$ close, initiating the discharge mode. This mode continues until the link current reaches the discharge reference current, I_{dis_ref} . This reference is designated to leave enough energy within the resonant tank in order to transition from the discharge mode to the charge mode as well as to ensure enough power is delivered to the load. This value is derived simply by dividing the power reference by the reference voltage value. The power reference is the power capacity of the converter.

After the discharge mode, the converter resonates again to facilitate soft switching on source 2's side. The rest of the diagram in Figure 4.4 follows the same guidelines as the logic already discussed. Once the voltage at the resonant tank and the filters on source 2's side are equal and the potential voltage difference between the two equivalent circuits are zero, switches $S2$ and $S4$ close. With this action, the converter charges the resonant tank in a negative direction.

Subsequent modes follow the same principles as for previous modes, however, the polarities of the current and voltage values are reversed.

It is imperative for the modulation switching sequence to charge and discharge the resonant tank in a way that the AC-link current oscillates positive and negative. This is executed with continuous monitoring of the tank's voltage and current, to then compare these values to the references as discussed earlier. This ensures that the tank acquires the AC-like dynamics. This point-by-point operating method benefits from instantaneous transfer between operating conditions, which makes it a very strong method for dealing with transient event-prone systems.

The AC-link circuit adapts instantaneously to the direction of power flow by continuously monitoring the terminals of the converter where the power is being consumed. That value is compared to a reference power value and from that error, a current reference is chosen within the link to optimally close and open specific switches. By monitoring the current through the resonant tank and comparing it with its reference value, the proper amount of energy will be distributed from the tank to the infinite bus. The tank then can transition from the discharge mode to the charge mode.

The logic for the system lets the converter operate in both directions, but to physically permit bidirectional power flow; two IGBT switches are paired together with antiparallel diodes. Unlike the dual active bridge converter, the AC-Link topology requires the additional switch to block current during the resonating cycles. This is to ensure no power is distributed to any of the branches in the converter during any of the modes unless the switches are activated. The logic monitors which direction the user wants the converter's power to flow at the end of each cycle. When the direction changes, so does the switching sequence to allow for a streamlined adjustment of directional current flow.

5.0 SIMULATION RESULTS AND DISCUSSION

This section discusses the results of the bidirectional dc-dc AC-link converter in both modes of operation utilizing state plane trajectory control. It also shows the response of the converter during both buck and boost modes during load induced transients. The parameters of the system are listed in Table 2. The resonant LC tank parameters were adapted from [11]. The control for the bidirectional power flow simulation is purely based off the logic from Figure 4.4.

Table 2: Converter parameters for bidirectional simulations

Symbol	Quantity	Value
$V_{\text{source 1}}$	Voltage Source 1	380 V _{dc}
$V_{\text{source 2}}$	Voltage Source 2	100 V _{dc}
f_{res}	Resonant Frequency	41.1 kHz
C_1 and C_2	Voltage Source 1 and 2 Capacitor Filters	100 μF
L_1 and L_2	Voltage Source 1 and 2 Inductor Filters	1 μH
L_r	Resonant Inductor	150 μH
C_r	Resonant Capacitor	0.1 μF
P_{ref}	Power Reference	1 kW

Since the converter operates around specific points in accordance with the resonant tank, it is essential to explain Figure 5.1. Shown in Figure 5.1, the IGBTs input gate signals are shown

along with the voltage and current waveforms from the AC-link. The modes of operation are shown at the bottom of the graphic. For this scenario, power is flowing from source 2 to source 1, in reference to the circuit in Figure 1.1.

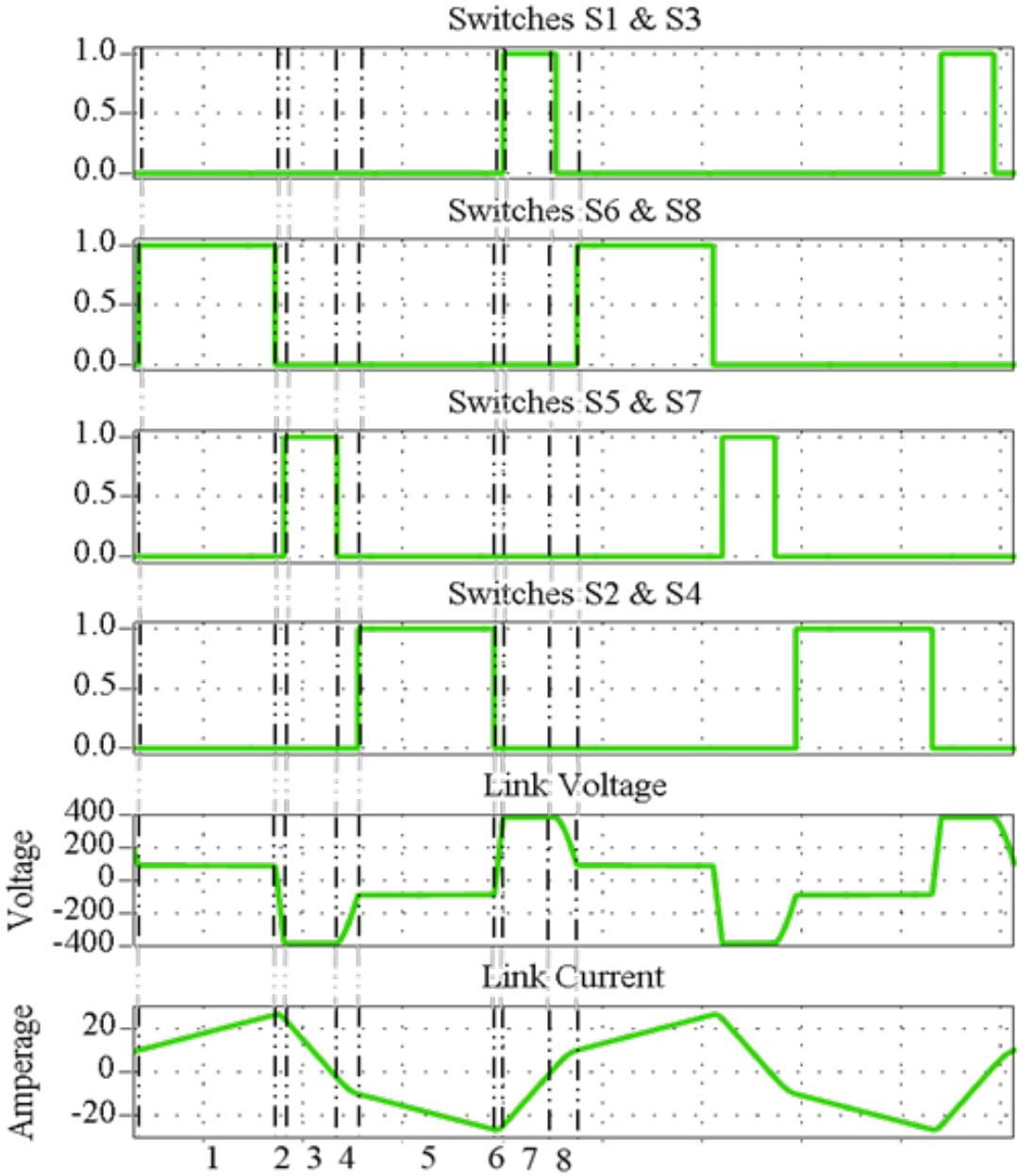


Figure 5:1: Switching Schemes for IGBTs with resonant tank voltage and current waveforms for boost operation

During mode 1, the converter is charging the resonant tank in a positive direction by closing switches $S6$ and $S8$. The resonant tank's capacitor voltage equals source 2's voltage and the current begins to linearly increase until it reaches its reference value, which will initiate the first resonant operation, mode 2.

While in the resonating mode, the AC-link oscillates and the LC tank transfers energy from the inductor to the capacitor, causing a build-up of voltage on the capacitor. This phenomenon relates to (2.27). Once the voltage across the resonant capacitor reaches source 1's voltage, the switches on source 1's side ($S5$ and $S7$) close with zero volts across the switches, initiating mode 3. During mode 3, the voltage on the resonant capacitor remains equal to source 1, and the current is discharged in the negative direction into the infinite bus.

Once the AC-link is fully discharged, the next resonant cycle begins, mode 4. As seen in Figure 5.1, the absolute-value voltage peak during mode 4 is much less than for mode 2 or mode 6. This occurs because the initial conditions for the resonant capacitor and inductor after the discharging cycle begin with less contained energy than the initial conditions after the charging cycle.

During the charging modes, 1 and 5, the gate inputs for the switches have a longer duty cycle than for the discharging modes 3 and 7. The longer duty cycle for the charging modes is attributed to source 2 naturally requiring a longer duration to reach its current reference point.

Figure 5.2 shows source 1's voltage and current, and source 2's voltage and current during operation. From 0 seconds to 0.03 seconds the converter is sending power from source 1 to source 2, which means the converter is in buck mode. Since it is now operating in buck mode, the converter must maintain the proper power value at source 2's terminals. The current and voltage at source 2 adjusts to maintain the power reference, while source 1 also adjusts to

support the load conditions. At 0.03 seconds, the converter switches the direction of the power flow, where the power is now flowing from source 2 to source 1, boost mode. Now, the converter adjusts the current and voltage at source 1 to maintain the reference power level, while source 2 adapts to the new change in load conditions.

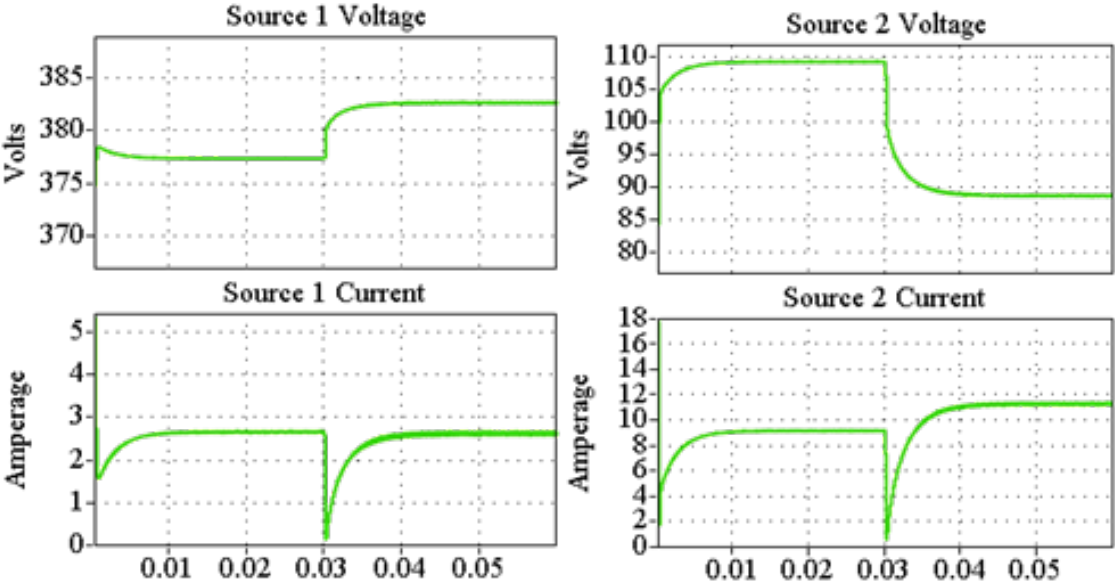


Figure 5:2: Source 1 and source 2 RMS voltage and current waveforms with different directions of power flow

Figure 5.3 displays the state plane trajectories for the converter during the same operation. The trajectories match the theoretical prediction shown in Figure 4.1 and Figure 4.2. The important characteristic in this trajectory to note is the change of the current value for each graphic. This is critical because it shows the circuit adapting to the change for the new power flow direction. The state plane trajectories for each direction of power flow complement each other in shape. This is expected as the same voltage requirements and power reference are the same for each condition.

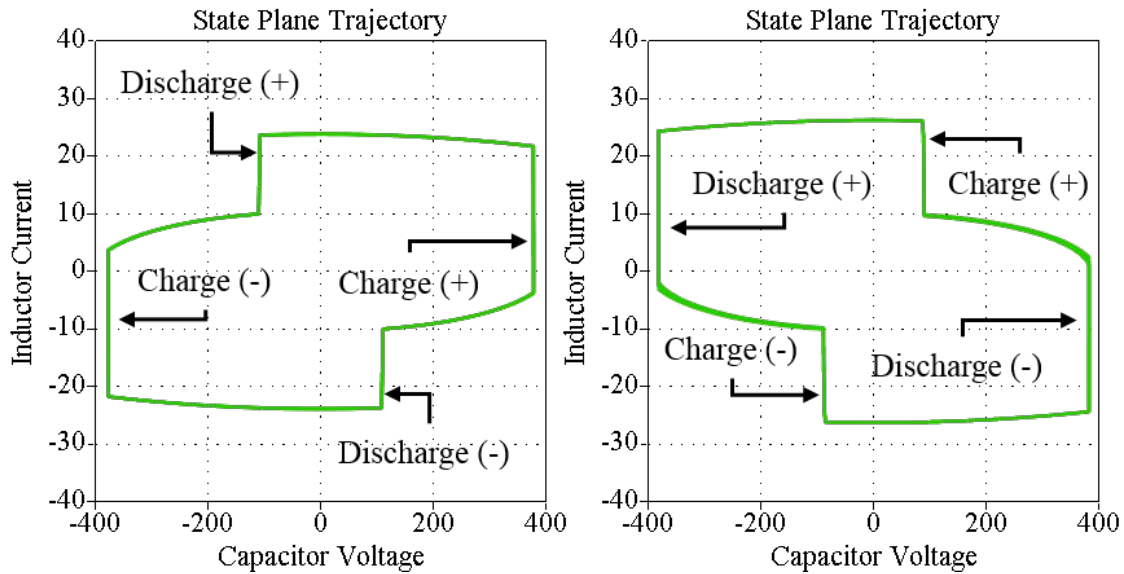


Figure 5.3: State plane trajectories for buck and boost modes of operation

The resonant modes enable the converter to achieve soft switching. The resonant transitions for the AC-Link shown in Figure 5.3, display that the modes of operation for the converter transition at source 1 and source 2's voltage values. This allows the converter to close the corresponding switches with zero voltage potential across the devices, effective ZVS. This feature equips the converter to operate at high switching frequencies.

5.1 SIMULATIONS FOR TRANSIENT EVENTS IN BOOST MODE

This section discusses the results of the dc-dc AC-link converter in boost mode during different load and input variations utilizing state plane trajectory control. The component parameters are the same as Table 2. The transient induced test parameters are listed below in Table 3.

Table 3: Simulation conditions for boost mode in transient events

Condition 1 (0s – 0.03s)		
$V_{\text{source 1}}$	Voltage Source 1	380 V _{dc}
$V_{\text{source 2}}$	Voltage Source 2	100 V _{dc}
Condition 2 (0.03s – 0.05s)		
$V_{\text{source 1}}$	Voltage Source 1	380 V _{dc}
$V_{\text{source 2}}$	Voltage Source 2	150 V _{dc}
Condition 3 (0.05s – 0.07s)		
$V_{\text{source 1}}$	Voltage Source 1	400 V _{dc}
$V_{\text{source 2}}$	Voltage Source 2	150 V _{dc}

These test conditions adjust the voltages on the two sources at three different instances. This will show the quick dynamic response of SPTC for sending power from source 2 to source 1 in the AC-link converter. It is important to display these conditions to validate SPTC functions properly in more than one scenario.

For this simulation, the converter starts out in *Condition 1*. This condition creates the initial startup. Then once *Condition 2* occurs, the sending source side, source 2, increases to 150 V_{dc}. After this occurs the AC-link converter adapts abruptly to the source value adjustment. However, when *Condition 3* occurs, the absorbing source, source 1, shifts to 400 V_{dc}. This load adjustment is corrected through an adjustment for the PI controller to meet the desired power reference at the absorbing source end. Nevertheless, the SPTC method is able to regulate the converter instantaneously to bring the measured values back to its anticipated ratings. This is the merit of using a control method like SPTC. By measuring the circuit's values and having specific

points of operation the converter operates around, creates a fast acting control system, especially in transient events.

Another important test is to ensure the converter's LC circuit drives the voltage to zero across the switch before closing the semiconductor in boost mode. Figure 5.4 shows the corresponding IGBTs along with the switches gate inputs in *Condition 3*. By observing the figure, it is shown that the voltage falls to zero volts, or is at zero volts, before the gate input turns on. By relating back to Figure 1.3, referring soft switching, the converter is operating with ZVS in ideal conditions. This is important because this is the first step to ensure the converter can operate at high frequencies in real-world applications without damaging the devices from heat, at least when switching losses are concerned. However, section 6.0 will display the non-ideal voltage and current waveforms on the switches with thermal models of the semiconductors implemented to further prove ZVS.

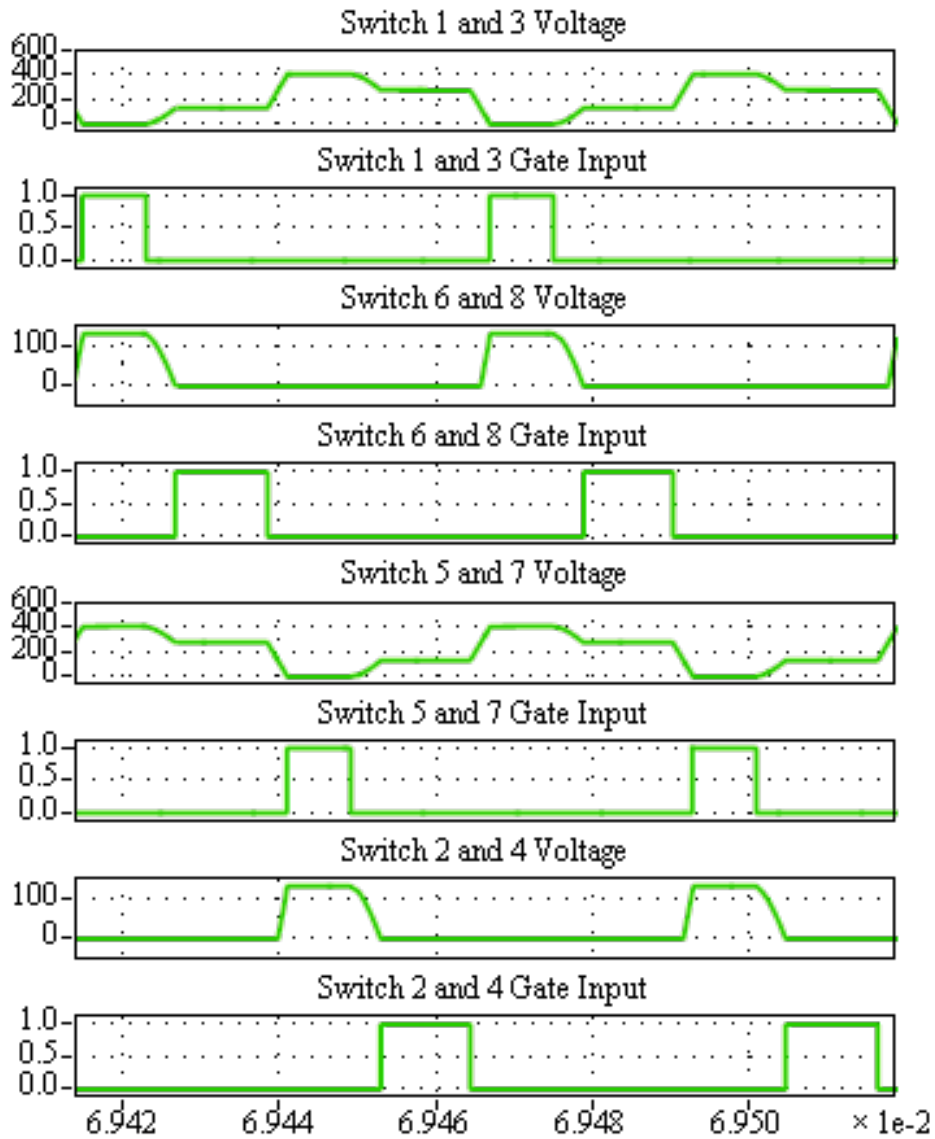


Figure 5.4: Switching Schemes for IGBTs displaying ZVS in *condition 3* during boost mode

Figure 5.5 shows the state plane trajectory for boost mode with the different corresponding transient conditions. It is important to note the change in current and voltage when the conditions take place. When the voltage rating drops (cond. 1 to cond. 2) the current reduces from about 27 A to 20A. This is to maintain the power rating on source 1 (absorbing end). The voltage can be seen to adjust with the different conditions. Cond. 2 and Cond. 3 maintain the same current levels because source 2 remains the same, while when source 1 adjusts to a higher

value, the voltage level also adjusts, as seen in Figure 5.5. The same test was compiled for the buck scenario, or power flowing from source 1 to source 2. This is shown in Figure 5.6, where the same three different case scenarios are shown. These descriptive trajectories prove that SPTC, or the point-to-point logic, is working as expected.

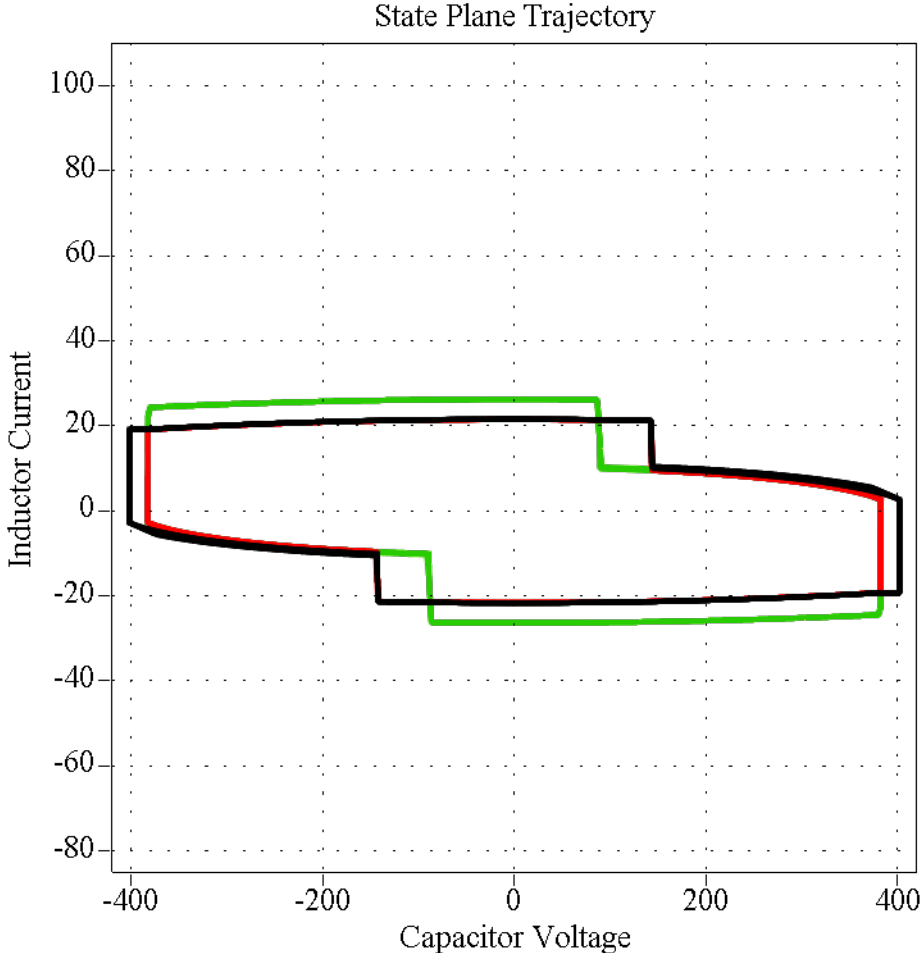


Figure 5:5: State Plane Trajectory for AC-Link resonant tank’s recovery after transient events during *boost* mode (green – cond. 1, red – cond. 2, black – cond. 3)

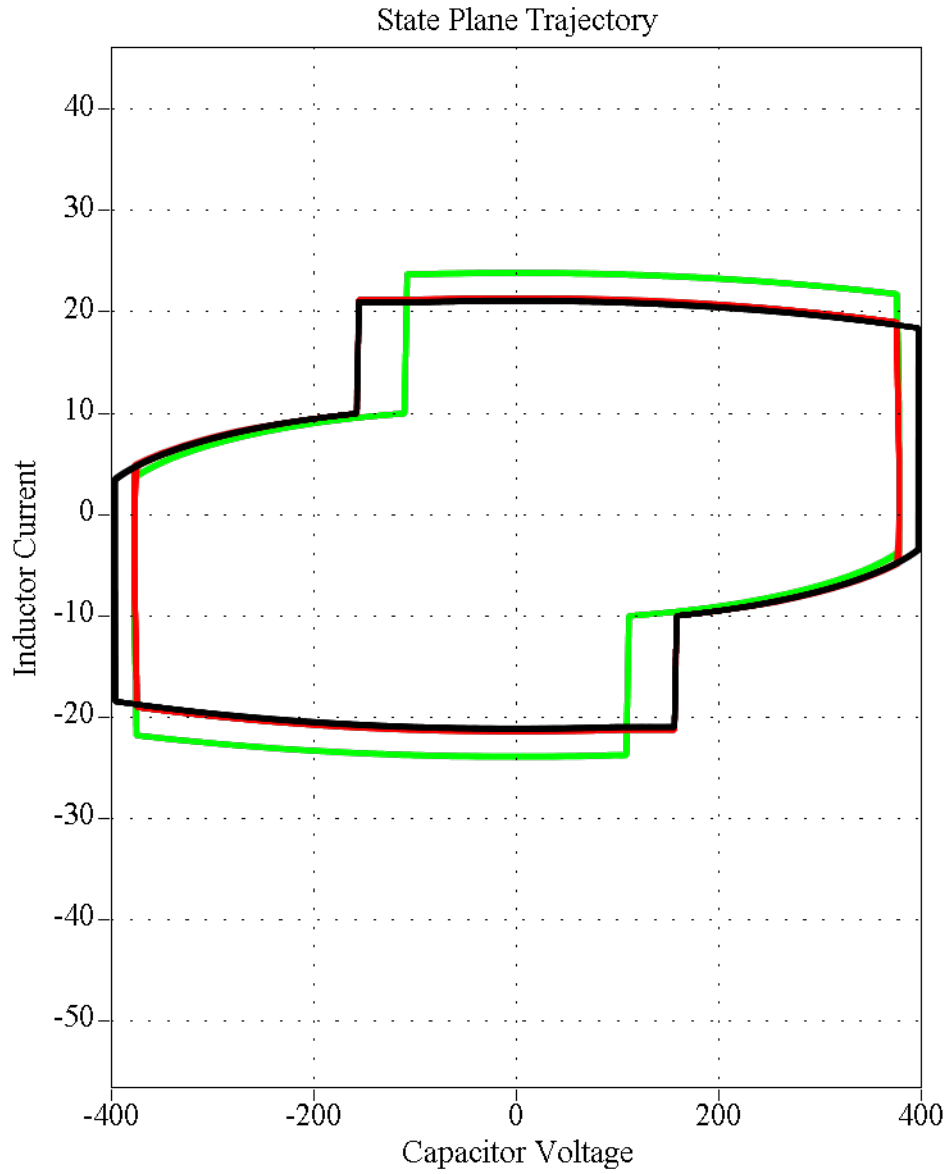


Figure 5:6: State Plane Trajectory for AC-Link resonant tank's recovery after transient events during *buck* mode (green – cond. 1, red – cond. 2, black – cond. 3)

6.0 THERMAL RESPONSE IN DC-DC AC-LINK CONVERTER USING SPTC

To further validate the AC-link converter can be constructed without damaging semiconductor and passive elements, a detailed thermal analysis for the converter and the control technique need to be simulated. The results shown are from the buck test case due to the similarity of both directions of power flow. The boost modes results are similar to the buck mode of operation.

These simulations will also be able to show if the converter is achieving zero voltage switching and the temperature the semiconductors operate around. The simulation took place using ANSYS Simplorer. This simulation tool is accurate due to the ability to select real components through finding appropriate data sheet information and implementing thermal curves from the data sheet into ANSYS Simplorer. The corresponding information for the simulations are presented in Table 5 where the thermal information for the IGBT is from *Infineon*.

It is equally important to see if there are large temperature swings within the semiconductor devices. Temperature swings can have devastating effects on the semiconductor devices. When it comes to temperature, the longevity of switches can expanded if the temperature remains constant, even if it is a high temperature, compared to an ever-fluctuating temperature across the switch [28]. An analogy of this can be compared to asphalt in a climate that has all four seasons compared to a constant warm climate. The expanding and contracting of

the asphalt (expanding and contracting of physical material on device) will cause defects in the road (semiconductor).

Table 4: Converter parameters for thermal analysis for AC-link converter

Parameter	Description	Values
$V_{\text{source 1}}$	Voltage Source 1	380 V _{dc}
$V_{\text{source 2}}$	Voltage Source 2	100 V _{dc}
f_{res}	Resonant Frequency	41.1 kHz
C_1 and C_2	Voltage Source 1 and 2 Capacitor Filters	100 μF
L_1 and L_2	Voltage Source 1 and 2 Inductor Filters	1 μH
L_r	Resonant Inductor	150 μH
C_r	Resonant Capacitor	0.1 μF
P_{ref}	Power Reference	1 kW
S_n	Main Switches (IKW50N60DTP)	IGBT, 50 A, 600V, $V_{\text{CE(sat)}} = 1.6 \text{ V}$

6.1 THERMAL MODELING OF CONVERTER IN BUCK MODE

Because operation of the converter is very similar in buck and boost modes, this section will only discuss certain cases for the buck mode, or power flowing from source 1 to source 2. To further validate the operation of the SPTC logic proposed in this literature, zero voltage switching needs to be proven in a realistic case with non-ideal components. The logic from Figure 4.4 is implemented in ANSYS along with the same circuit from Figure 1.1. The simulation tool is also able to provide realistic thermal data. The thermal information from the semiconductor devices is

useful in determining the overall effectiveness of the control logic in response to losses in the system.

Figure 6.1, Figure 6.2, Figure 6.3, and Figure 6.4 provides the voltage, current, and gate input waveforms. These waveforms are crucial to validating the operation of the converter with zero voltage switching at the closing point of the switch. If there were any significant amount of voltage remaining on the switch, large current spikes would be present in the aforementioned figures at the closing point of the switch. Current spikes can be prevalent in resonant circuits especially if the resonant circuit is abruptly interrupted. This is because a tremendous amount of energy can be stored in the LC circuit and when disturbed in a non-controlled fashion, the energy is discharged rapidly from the capacitor.

Figure 6.5 shows the temperature plot of the recorded switches. This shows the switches remain at a normal operating temperature throughout utilizing SPTC. The temperature plot's Y axis is in Celsius where 25 C is considered room temperature. The maximum point of temperature at steady state is recorded at switches 2, 4, 6, and 8 at 26.50 C. Even though that is the highest point of stress for the switches, the switches all operate within approximately 1 C of each other. SPTC proves to keep the temperature of the switches considerably low instead of high with large fluctuations, which will effectively increase the longevity of the semiconductor devices.

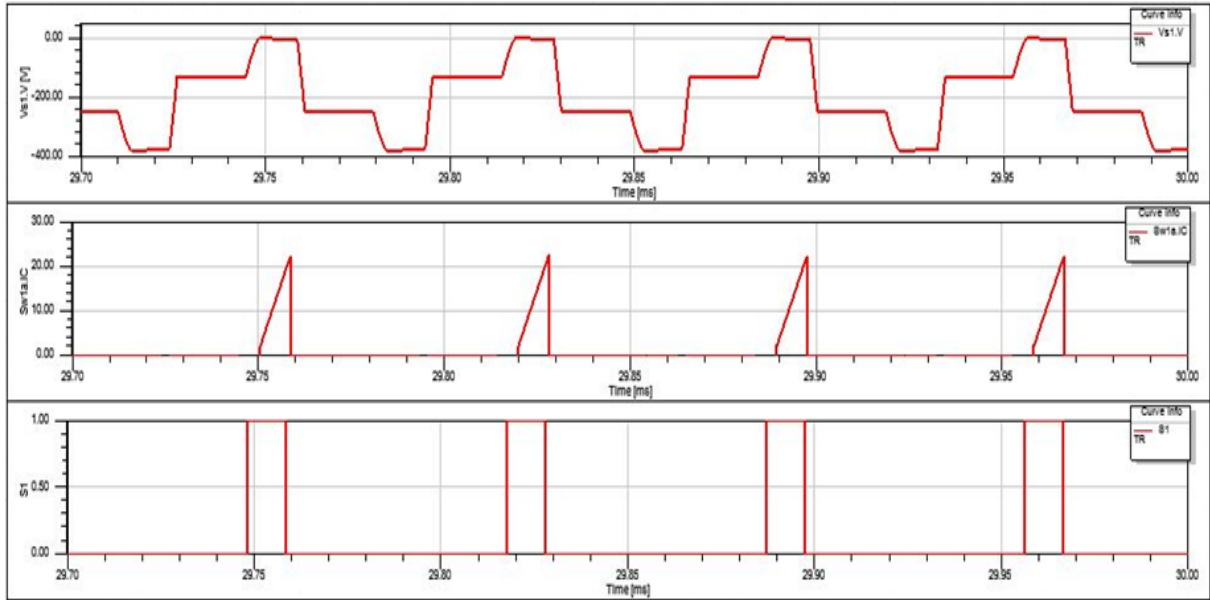


Figure 6:1: Switch 1 and Switch 3's voltage, current, and gate input waveforms in buck mode

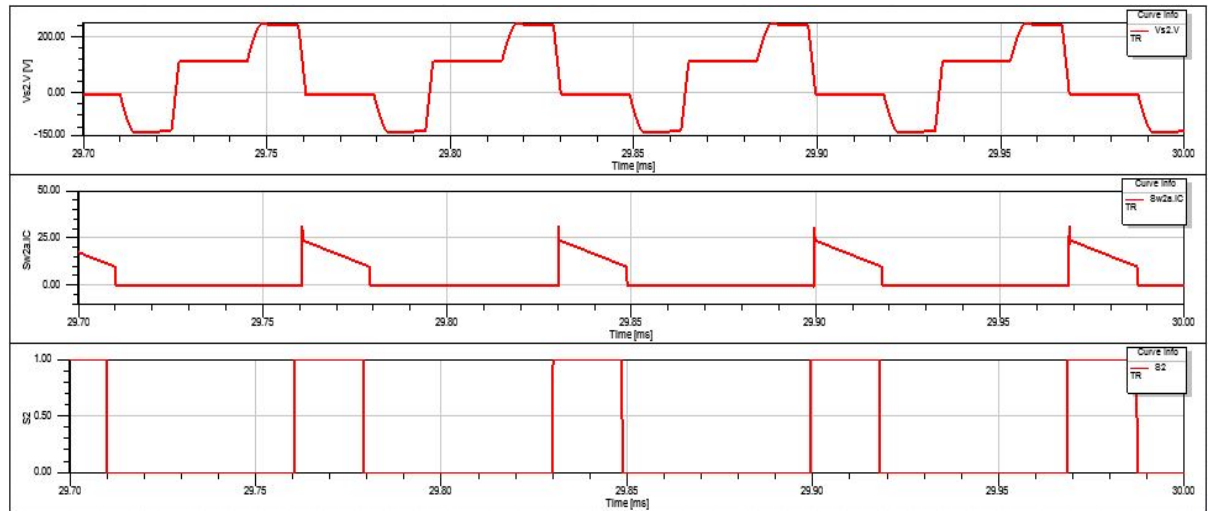


Figure 6:2: Switch 2 and Switch 4's voltage, current, and gate input waveforms in buck mode

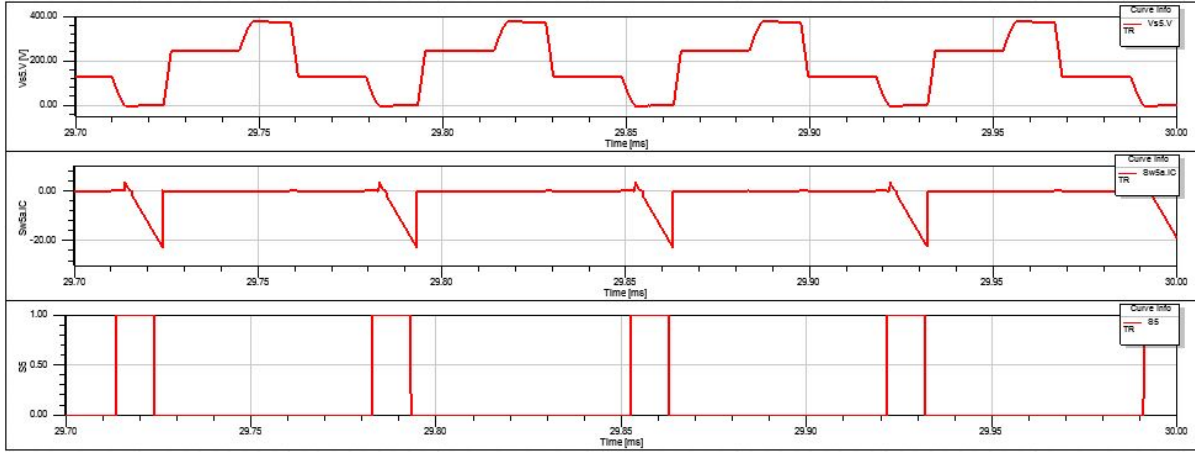


Figure 6:3: Switch 5 and Switch 7's voltage, current, and gate input waveforms in buck mode

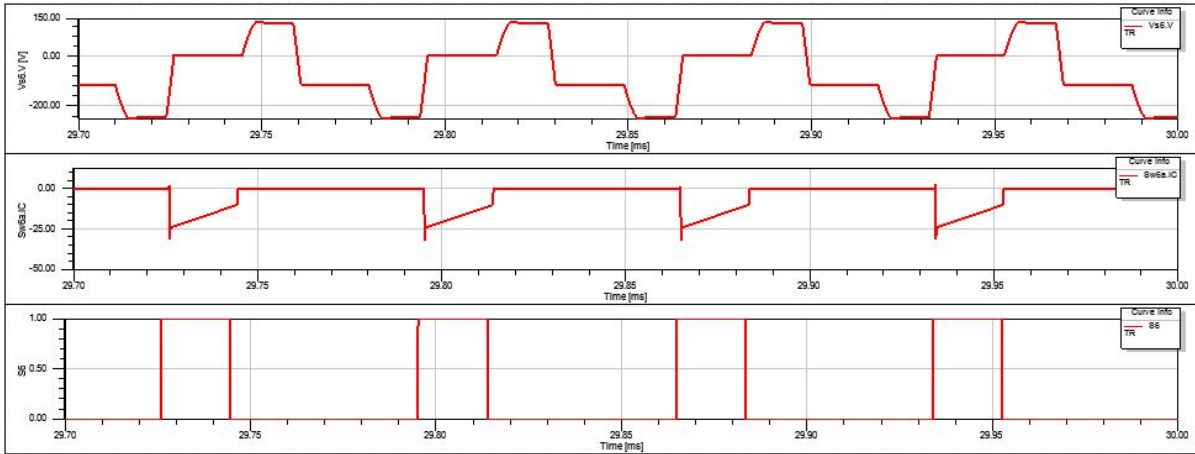


Figure 6:4: Switch 6 and Switch 8's voltage, current, and gate input waveforms in buck mode

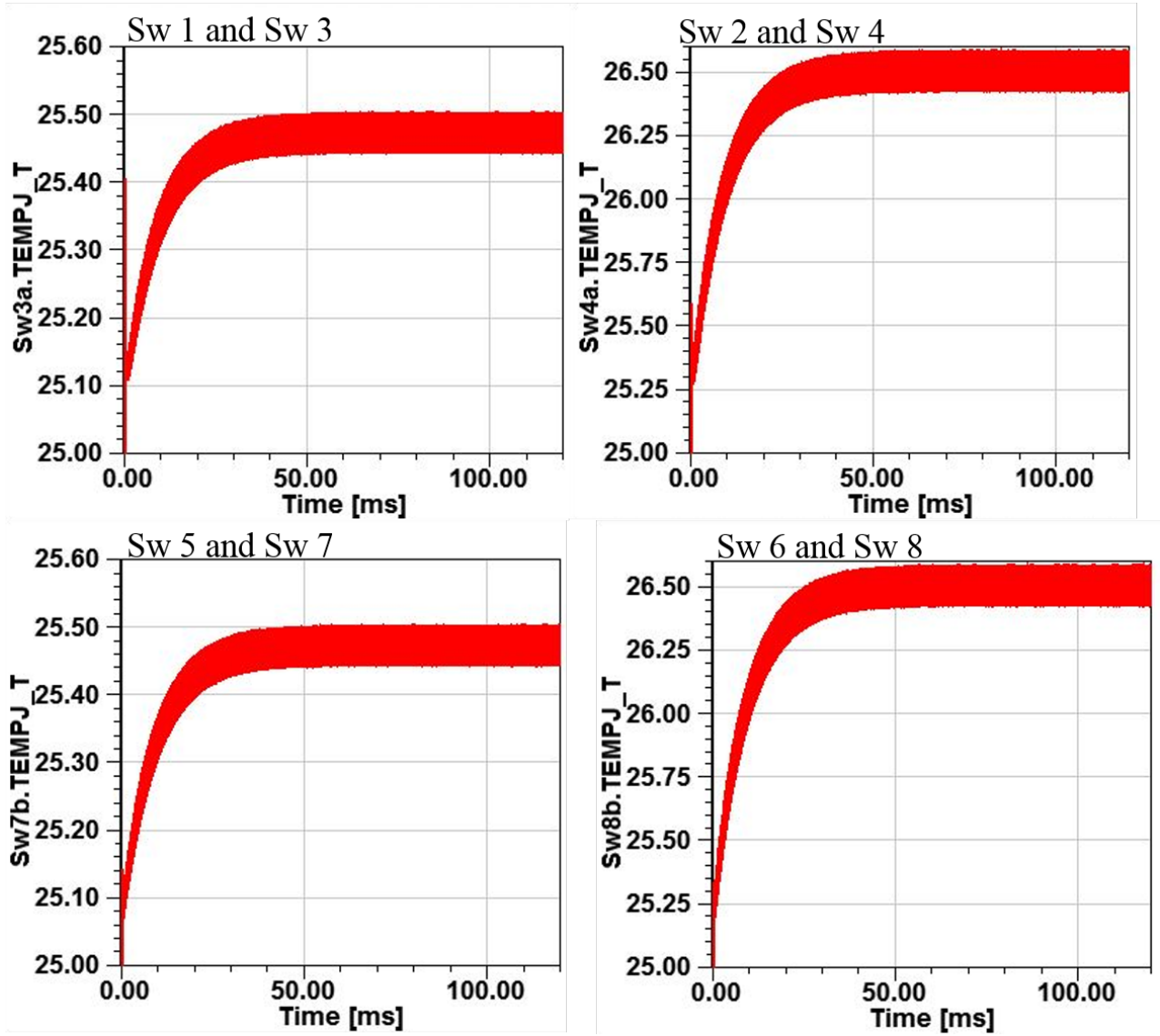


Figure 6:5: Temperature plots for the IGBTs during buck mode

7.0 CONCLUSION

This document provides sufficient background information on the dc-dc AC-link converter and similar topologies and control methods. In addition, this paper provides the mathematical analysis for the AC-link converter utilizing state plane analysis. The SPTC logic proposed for this converter was developed utilizing knowledge from state plane analysis to lower voltage stress on the devices using soft switching techniques. The proposed SPTC was implemented by use of a state machine, supporting bidirectional power flow, simply requiring the voltage and current state variable measurements of the resonant tank. A detailed thermal analysis study for this converter was conducted to prove zero voltage switching was achieved. It also provides the framework for prototyping the converter for real-world test scenarios.

BIBLIOGRAPHY

- [1] W. Alexander, "Universal power converter." US patent 2008/0013351A1, 2008.
- [2] M. Amirabadi, "Soft-Switching High-Frequency AC-Link Universal Power Converters with Galvanic Isolation," Texas A&M University, 2013.
- [3] B. Zhao, Q. Song, W. Liu, and Y. Sun, "Overview of dual-active-bridge isolated bidirectional DC-DC converter for high-frequency-link power-conversion system," *IEEE Trans. Power Electron.*, vol. 29, no. 8, pp. 4091–4106, 2014.
- [4] D. Costinett, D. Maksimovic, and R. Zane, "Design and control for high efficiency in high step-down dual active bridge converters operating at high switching frequency," *IEEE Trans. Power Electron.*, vol. 28, no. 8, pp. 3931–3940, 2013.
- [5] F. Caricchi, F. Crescimbin, F. G. Capponi, and L. Solero, "Study of bi-directional buck-boost converter topologies for application in electrical vehicle motor drives," *APEC '98 Thirteen. Annu. Appl. Power Electron. Conf. Expo.*, vol. 1, pp. 287–293, 1998.
- [6] J. Chen, D. Maksimović, and R. Erickson, "Buck-boost PWM converters having two independently controlled switches," *PESC Rec. - IEEE Annu. Power Electron. Spec. Conf.*, vol. 2, pp. 736–741, 2001.
- [7] G. Stahl, M. Rodriguez, and D. Maksimovic, "A high-efficiency bidirectional buck-boost DC-DC converter," *Conf. Proc. - IEEE Appl. Power Electron. Conf. Expo. - APEC*, pp. 1362–1367, 2012.
- [8] M. Agostinelli, R. Priewasser, S. Marsili, and M. Huemer, "Fixed-frequency pseudo sliding mode control for a buck-boost DC-DC converter in mobile applications: A comparison with a linear PID controller," *Proc. - IEEE Int. Symp. Circuits Syst.*, pp. 1604–1607, 2011.
- [9] T. Wang, S. Sen, and M. Amirabadi, "Soft switching high frequency AC-link DC-DC buck-boost converters," *Conf. Proc. - IEEE Appl. Power Electron. Conf. Expo. - APEC*, vol. 2015–May, no. May, pp. 57–64, 2015.
- [10] M. Amirabadi, H. A. Toliyat, and W. C. Alexander, "Single-phase soft-switching AC-link buck-boost inverter," *Conf. Proc. - IEEE Appl. Power Electron. Conf. Expo. - APEC*, pp. 2192–2199, 2014.

- [11] G. M. Dousoky, M. Mosa, and H. Abu-Rub, "Single-phase ZVS bidirectional AC-link converter for EV batteries-grid integration," *2014 IEEE Energy Convers. Congr. Expo. ECCE 2014*, pp. 2532–2537, 2014.
- [12] K. George, "Design and Control of a Bidirectional Dual Active Bridge DC-DC Converter to Interface Solar , Battery Storage , and Grid-Tied Inverters," University of Arkansas, 2015.
- [13] H. Wang and F. Blaabjerg, "Reliability of capacitors for DC-link applications in power electronic converters—an overview," *IEEE Trans. Ind. Appl.*, vol. 50, no. 5, pp. 3569–3578, 2014.
- [14] R. W. Erickson and D. Maksimovic, *Fundamentals of Power Electronics*, 2nd ed. Norwell, Mass: Kluwer Academic Publishers, 2004.
- [15] M. M. Ghahderijani, M. Castilla, A. Momeneh, J. T. Miret, and L. G. De Vicuna, "Frequency-Modulation Control of a DC/DC Current-Source Parallel-Resonant Converter," *IEEE Trans. Ind. Electron.*, vol. 64, no. 7, pp. 5392–5402, 2017.
- [16] M. Kim and M. Youn, "an Energy Feedback Control of Series Resonant Converter," *Sci. Technol.*, vol. 6, no. 3, pp. 59–66, 1990.
- [17] D. J. Tschirhart and P. K. Jain, "A CLL Resonant Asymmetrical With Improved Efficiency," *IEEE Trans. Ind. Electron.*, vol. 55, no. 1, pp. 114–122, 2008.
- [18] M. Castilla, S. Member, and S. Member, "On the Design of Sliding Mode Control Schemes for Quantum Resonant Converters," *IEEE Trans. Power Electron.*, vol. 15, no. 6, pp. 960–973, 2000.
- [19] E. L. Henk Huisman, Furkan Bas¸kurt, Apostolos Bouloukos, Nico Baars, "Optimal Trajectory Control of a Series-Resonant Inverter with a Non-Linear Resonant Inductor," *IEEE Int. Symp. Predict. Control Electr. Drives Power Electron.*, pp. 54–59, 2017.
- [20] A. Sabanovic, "Variable Structure Systems With Sliding Modes in Motion Control—A Survey," *IEEE Trans. Ind. Informatics*, vol. 7, no. 2, pp. 212–223, 2011.
- [21] M. Moradi Ghahderijani, M. Castilla, A. Momeneh, J. Miret, and L. García de Vicuña, "Robust and fast sliding-mode control for a DC–DC current-source parallel-resonant converter," *IET Power Electron.*, vol. 11, no. 2, pp. 262–271, 2018.
- [22] R. Venkataramanan, "Sliding Mode Control of Power Converters," California Institute of Technology, 1986.
- [23] R. Oruganti and F. C. Lee, "Resonant Power Processors, Part II-Methods of Control," *IEEE Trans. Ind. Appl.*, vol. IA-21, no. 6, pp. 1461–1471, 1985.

- [24] W. Feng, F. C. Lee, D. J. Stilwell, and A. L. Wicks, "State-Trajectory Analysis and Control of LLC Resonant Converters," Virginia Polytechnic Institute and State University, 2013.
- [25] B. Fincan, T. N. Guzin, and M. Biberoglu, "Extending the state plane analysis of parallel resonant converter by incorporating several non-ideality sources," *2016 18th Eur. Conf. Power Electron. Appl. EPE 2016 ECCE Eur.*, 2016.
- [26] W. Feng, F. C. Lee, and P. Mattavelli, "Simplified Optimal Trajectory Control (SOTC) for LLC Resonant Converters," *IEEE Trans. Power Electron.*, vol. 28, no. 5, pp. 2415–2426, 2013.
- [27] G. G. Oggier, M. Ordonez, J. M. Galvez, and F. Luchino, "Fast transient boundary control and steady-state operation of the dual active bridge converter using the natural switching surface," *IEEE Trans. Power Electron.*, vol. 29, no. 2, pp. 946–957, 2014.
- [28] P. T. Lewis, B. M. Grainger, and S. Huang, "Silicon and SiC MOSFET Electro-Thermal Performance Assessment within Smart Distributed Generation Inverters with Dynamic Reactive Compensation Grid Support for Resilient Microgrids," *2017 IEEE 18th Work. Control Model. Power Electron. COMPEL 2017*, 2017.